



# Immediate propagation of deglacial environmental change to deep-marine turbidite systems along the Chile convergent margin



Anne Bernhardt<sup>a,b,\*</sup>, Wolfgang Schwanghart<sup>b</sup>, Dierk Hebbeln<sup>c</sup>, Jan-Berend W. Stuut<sup>c,d</sup>, Manfred R. Strecker<sup>b</sup>

<sup>a</sup> Institute of Geological Sciences, Freie Universität Berlin, Germany

<sup>b</sup> Institute of Earth and Environmental Science, Potsdam University, Germany

<sup>c</sup> MARUM – Center for Marine Environmental Sciences, University of Bremen, Germany

<sup>d</sup> NIOZ – Royal Netherlands Institute for Sea Research, Department of Ocean Systems, and Utrecht University, Texel, The Netherlands

## ARTICLE INFO

### Article history:

Received 28 July 2016

Received in revised form 11 May 2017

Accepted 14 May 2017

Available online xxxx

Editor: H. Stoll

### Keywords:

signal propagation

turbidity currents

Chile

sediment-routing system

connectivity

Last Glacial Maximum

## ABSTRACT

Understanding how Earth-surface processes respond to past climatic perturbations is crucial for making informed predictions about future impacts of climate change on sediment fluxes. Sedimentary records provide the archives for inferring these processes, but their interpretation is compromised by our incomplete understanding of how sediment-routing systems respond to millennial-scale climate cycles. We analyzed seven sediment cores recovered from marine turbidite depositional sites along the Chile continental margin. The sites span a pronounced arid-to-humid gradient with variable relief and related sediment connectivity of terrestrial and marine environments. These sites allowed us to study event-related depositional processes in different climatic and geomorphic settings from the Last Glacial Maximum to the present day. The three sites reveal a steep decline of turbidite deposition during deglaciation. High rates of sea-level rise postdate the decline in turbidite deposition. Comparison with paleoclimate proxies documents that the spatio-temporal sedimentary pattern rather mirrors the deglacial humidity decrease and concomitant warming with no resolvable lag times.

Our results let us infer that declining deglacial humidity decreased fluvial sediment supply. This signal propagated rapidly through the highly connected systems into the marine sink in north-central Chile. In contrast, in south-central Chile, connectivity between the Andean erosional zone and the fluvial transfer zone probably decreased abruptly by sediment trapping in piedmont lakes related to deglaciation, resulting in a sudden decrease of sediment supply to the ocean. Additionally, reduced moisture supply may have contributed to the rapid decline of turbidite deposition. These different causes result in similar depositional patterns in the marine sinks. We conclude that turbiditic strata may constitute reliable recorders of climate change across a wide range of climatic zones and geomorphic conditions. However, the underlying causes for similar signal manifestations in the sinks may differ, ranging from maintained high system connectivity to abrupt connectivity loss.

© 2017 Elsevier B.V. All rights reserved.

## 1. Introduction

In light of global change, understanding how the Earth's surface responds to climate forcing is increasingly important to make informed predictions about future environmental perturbations and their impact on sediment production and transport (Pelletier et al., 2015). As soon as predictions concern changes in the sediment-routing system related to millennial environmental changes, however, extrapolations beyond decadal to centennial

measurements from historic records may lack a conceptual basis (Brunsden and Thornes, 1979). Sedimentary records extend historical data sets and potentially reflect past environmental changes, but their interpretation is compromised by our incomplete understanding of how sediment supply (Qs) signals are generated in the initial erosional zone (Armitage et al., 2013; Godard et al., 2013; Braun et al., 2015; Garcin et al., 2017). Moreover, the details of how sediment sources and sinks are dynamically linked by a sediment-routing system that reliably transfers (Covault et al., 2010; Bonneau et al., 2014), buffers (Clift and Giosan, 2014), destroys (Jerolmack and Paola, 2010), modifies, or amplifies environmental signals (Simpson and Castellort, 2012), are crucial when interpreting sediment archives in the light of past up-

\* Corresponding author.

E-mail address: anne.bernhardt@fu-berlin.de (A. Bernhardt).

land changes (e.g., Romans et al., 2016; Hoffmann, 2015). This is particularly true for terrigenous sediment accumulations in the ultimate sink, the deep-marine realm, and their value for environmental reconstruction (e.g., Romans and Graham, 2013; Castellort et al., 2015).

In an ideal setting, environmental signals propagate through the sedimentary system from the erosional zone via a transfer zone to a depositional zone (Schumm, 1981). The transitions between these zones are not strict as they potentially all contribute to sediment production, transfer, and storage (e.g., Bracken et al., 2015). The concept of sediment connectivity describes the sediment transfer from all potential sources to all sinks through different geomorphic compartments and can be used to describe the continuity of sediment transfer in a sediment-routing system (e.g., Bracken et al., 2015). Connectivity is a three-dimensional property (longitudinal, lateral and vertical). Longitudinal connectivity includes upstream-downstream relationships and denotes the ability of a river to transfer or accumulate sediment; lateral connectivity denotes the supply of sediment to the river channel (hillslope-channel, channel-floodplain); and vertical connectivity links surface-subsurface interactions of water, sediment, and nutrients (Brierley et al., 2006). Furthermore, connectivity is subject to changes over time. Systems with a high degree of longitudinal connectivity can rapidly transmit environmental signals (Hoffmann, 2015). Lateral connectivity can act in two ways: coupling between rivers and floodplains can increase the sediment-residence time in the fluvial domain, whereas enhanced hillslope-river coupling can increase sediment transfer to the fluvial system (Heckmann and Schwanghart, 2013). Climate change such as aridification may decrease  $Q_s$  to the depositional zone (e.g., Syvitski et al., 2003) not only by lowering erosion rates, but also by decreasing inter- and intracompartamental connectivity (e.g., Jain and Tandon, 2010; Bracken et al., 2015). Intermediate sediment storage as a result of low connectivity may occur in alluvial fans, river floodplains, on the shelf and within submarine canyons (e.g., Hinderer, 2012; Allin et al., 2016).

The response time of a sedimentary system to any perturbation is determined by the response times of the associated erosion and transfer zones. The complexities of sediment transfer introduce time lags that may overlap with timescales of forcing signals and obliterate any signal to be recorded in the sink (Jerolmack and Paola, 2010; Coulthard and Van de Wiel, 2013). A classification of systems into 'reactive' and 'buffered', i.e. the period of the forcing is longer than the response time and vice versa (*sensu* Allen, 2008), may not fully embrace the complexities and potential pitfalls in interpretations of sedimentary records. Long response times of the erosional or transfer zones may result into a delayed or no recording of the forcing in the archive; however, a decrease in connectivity may lead to the same results.

Stratigraphic records in deep-marine sinks are complicated by changes of the shelf-transfer zone due to sea-level variations. However, turbidity currents form one of the volumetrically most important sediment-transport processes on Earth; e.g., a single turbidity current can transport >10 times the annual sediment flux from global fluvial systems (Talling et al., 2007). Turbidity-current frequencies have a wide range of implications as they affect the efficiency of organic carbon burial, and hence the global carbon cycle and related climate change (Galy et al., 2007), and pose severe hazards for important seafloor infrastructure (Carter et al., 2014). Furthermore, submarine fans represent the final sink of terrigenous sediments and are key locations for the quantification of land-to-sea sediment transfer at a global scale. A global comparison of deposition rates on submarine fans has shown that submarine flow activity is highly variable in time and not always directly linked to sea-level changes (Covault and Graham, 2010). During high sea level, inundated continental shelves can accommo-

date sediment, whereas under low sea-level conditions sediment can bypass the shelf. Thus, sea-level variations can modulate the connectivity between the transfer zone and deep-marine sink (e.g., Toucanne et al., 2012). Currents parallel to the shelf, however, can transport sediment into canyons that incise the shelf break and reduce the residence time of sediment on the shelf during sea-level highstands (e.g., Covault et al., 2007; Bernhardt et al., 2016). Few field studies investigated whether high-frequency climatic changes are reflected in the marine turbidite record (e.g., Toucanne et al., 2008, 2009, 2012; Ducassou et al., 2009; Romans et al., 2009; Covault et al., 2010; Bonneau et al., 2014; Clare et al., 2015). These studies suggest that low-order mountain rivers rapidly transfer sedimentary signals of millennial-scale climate cycles to the deep-marine record, especially if rivers connect to submarine canyons along narrow shelves (Romans et al., 2009; Covault et al., 2010; Bonneau et al., 2014). In contrast, large alluvial river systems draining onto wide shelves tend to buffer external signals (Métivier and Gaudemer, 1999) so that records of deep-marine sinks significantly lag upland erosion (Clift and Giosan, 2014). Whether fluvial routing systems buffer or rapidly react (*sensu* Allen, 2008) to environmental perturbations may also change through time. For example, Western European routing systems had a higher degree of connectivity during deglaciation than today due to lower base level (Toucanne et al., 2012).

Tracing the impact of climatic perturbations on deep-marine archives in regions with well documented climatic changes will improve our understanding of how environmental signals can be deconvolved in these ultimate sinks. In this study, we test how a deglacial humidity decrease propagates into clastic deposits along the Chile continental margin (Fig. 1). In particular, we investigate how the migration of the moisture-laden Southern Hemisphere Westerly Winds (SHWW) (e.g., Denton et al., 1999; Lamy et al., 1999) is reflected in the turbidite record of three sites at 30°S, 32.5°S and 38–40°S with contrasting present-day climates, topographic gradients, and thus different degrees of connectivity between sediment sources and sinks (Fig. 1). Therefore, we analyze deep-sea sediment cores containing turbidite successions from the Last Glacial Maximum (LGM) to the present and compare these to multiple climate proxies to determine lag times in the sediment-system response. With this approach, we tackle the following research questions:

1. How does an onshore decrease in humidity affect clastic sediment export to the deep ocean?
2. At what tempo is the climatic  $Q_s$  signal generated and transferred into the marine realm?
3. How do changing boundary conditions, such as onshore climate and system connectivity, affect signal propagation?

## 2. Regional setting

### 2.1. Tectonic setting, geomorphology and study sites

The Chile convergent margin features pronounced climatic and geomorphic gradients and well-documented paleoenvironmental changes, and thus provides an excellent test site for the investigation of climate-signal propagation to the ocean over the last glacial-interglacial cycle. We chose three sites offshore the presently arid (30°S, Site A), semiarid (32.5°S, Site SA), and humid (38–40°S, Site H) sectors of the Chile margin that represent a north-south decrease in average onshore topographic gradient and increase in shelf width (Figs. 1, 2). As turbidite records can be subject to authigenic processes (e.g., Wang et al., 2011), or render incomplete records due to bypass and erosion, we compiled the records of several cores at sites A and H to minimize the ef-

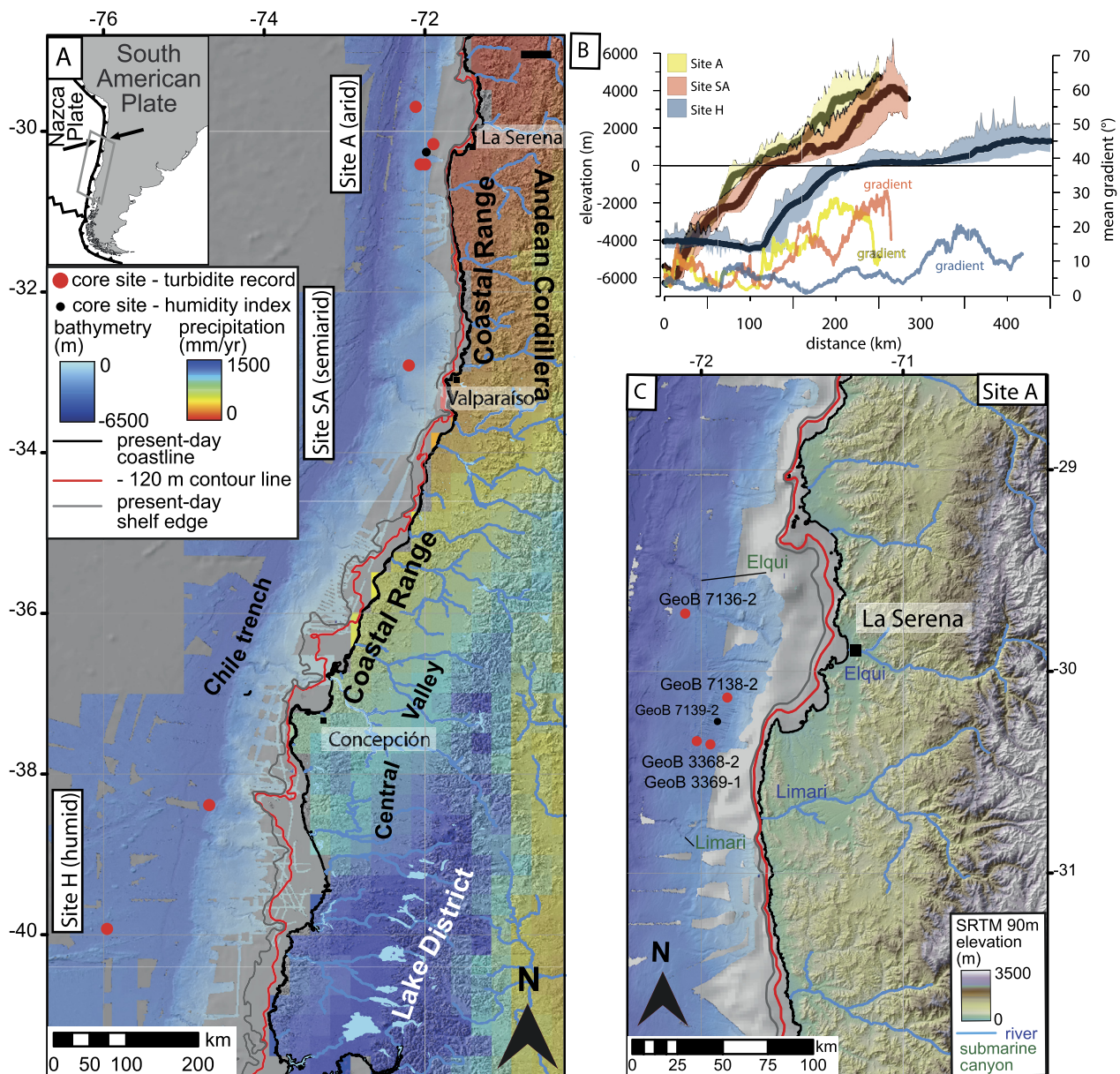


**Fig. 1.** Overview of the studied areas. (A) Overview map of the Chile margin section draped with the mean annual rainfall distribution derived from the Tropical Rainfall Measurement Mission (TRMM) satellite (courtesy of B. Bookhagen, Potsdam University). Bathymetry is compiled from several RV Sonne research cruises and is underlain by the hillslope-shade map derived from the Etopo1 database (<http://maps.ngdc.noaa.gov>). (B) Swath profiles across the three study sites showing mean, minimum and maximum elevations as well as mean gradients. (C–E) Close-up of the three study areas. Grey spots in bathymetry represent data gaps in the RV Sonne bathymetry which are filled by the Etopo1 hillshade map.

fects of local and intrinsic controls. Only one core from a turbidite depocenter was available from Site SA.

In north-central Chile (27–33°S), the onshore margin is characterized by the main Andean Cordillera that transitions westward into the Coastal Cordillera (Figs. 1B, 2A). A Central Valley in the upper plate is absent in this area, which is possibly related to flat-slab subduction (Jordan et al., 1983). Upland topographic gradients are steep and terrestrial sediment storage is limited. At the northern, arid study site (Site A), the shelf is narrow to absent (0–4 km) due to upper plate deformation related to basal subduction erosion (Contreras-Reyes et al., 2015) (Fig. 1A–C). Site A cores (Table 1) are located between 28 km and 70 km west of the coast at water depths between 2700 and 3500 m on a gently inclined intraslope terrace. The terrace is dissected by gullies in the upper reaches and is bounded to the north at 29.3°S by the Elqui submarine canyon (Fig. 1B) with the Elqui River as the closest fluvial

sediment source (Table A1). GeoB7136-2 was recovered from the canyon flank downslope of a small gully that may pirate the upper parts of large turbidity currents (>300 m thick). GeoB7138-2, 3369-1, and 3368-2 are located between the Elqui and the Limari rivers (Table A1) and may receive sediment from both sources. Due to the short transfer distances from source to sink and the high onshore ( $17 \pm 1^\circ$  mean gradient and  $1\sigma$  standard variation) and offshore ( $5 \pm 3^\circ$ ) topographic gradients (Figs. 1B, 2A), we infer a high degree of system connectivity at Site A.

The semiarid study site (Site SA) features a 6–17 km wide shelf (Figs. 1D, 2B). The upper slope is characterized by a forearc basin of ~50 km north-south width, the Valparaíso Basin, from which core GeoB3304-5 (Table 1) was retrieved 62 km west of the coastline at a water depth of 2411 m. To the north, the basin is fed by the La Ligua and Aconcagua submarine canyons (Laursen and Normark, 2003), which terminate ~15 km and ~21 km

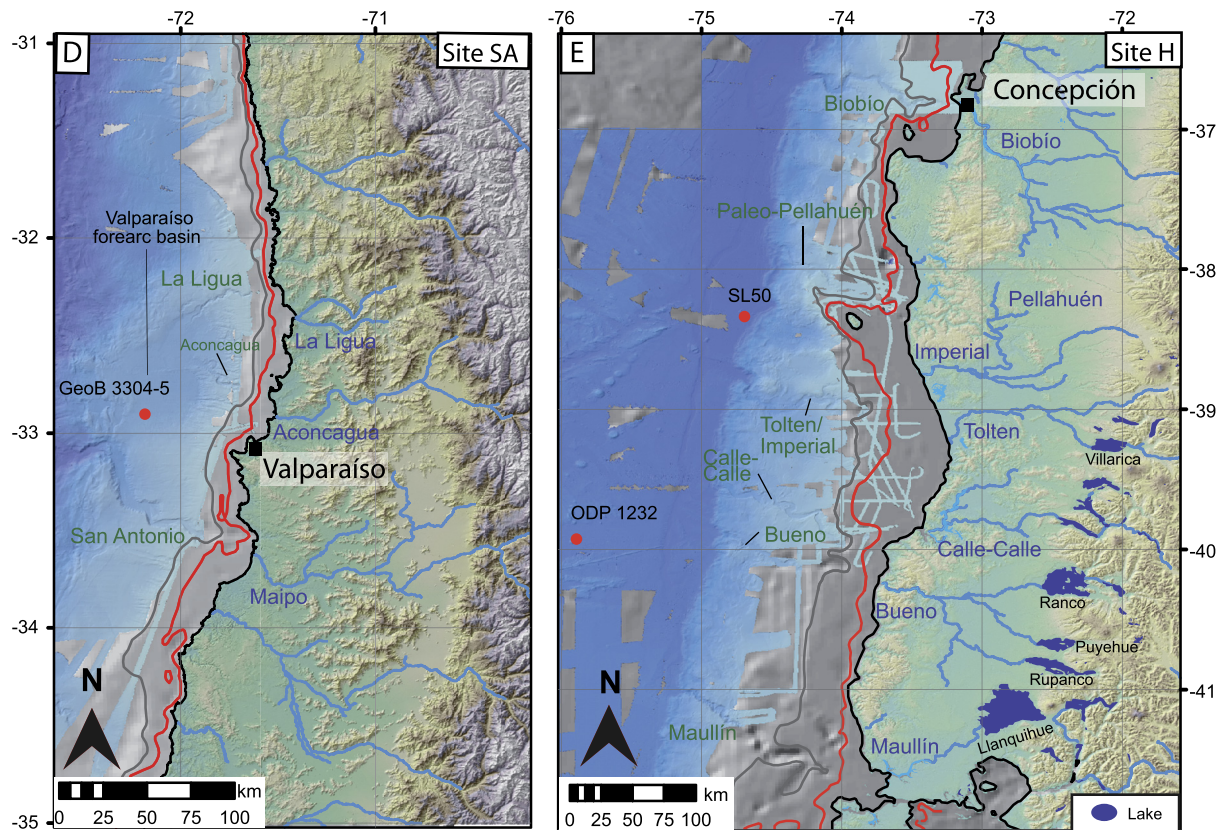


Fig. 1. (continued)

northwest of the responding river mouth, respectively. To the south, the forearc basin is bounded by the San Antonio Canyon (Laursen and Normark, 2002), which connects to the San Antonio river mouth (Fig. 1C). This canyon is >1 km deep and exhibits a meander bend at the longitude of GeoB3304-5 and very thick ( $\gg 1$  km), flow-stripped turbidity currents may have deposited turbidites at this core site. Site A and SA cores are recovered from low-gradient, non-channelized (at the resolution of the bathymetry: 100 m-grid-cell-size) areas, where the amount of erosion should be limited. Mean onshore and offshore gradients ( $18 \pm 7^\circ$  and  $6 \pm 3^\circ$ , respectively) at Site SA are comparable to Site A. Despite similar mean gradients, maps and swath-bathymetric profiles show potential intermediate sediment sinks along the routing system in low-grade intramontane areas, coast-proximal lowlands, and the narrow shelf (Figs. 1B–D, 2B). Hence, we infer the sediment-routing systems of Site SA to be well connected albeit to a somewhat lesser degree than those of Site A.

South of  $33^\circ\text{S}$ , the incoming plate subducts at an angle of  $30^\circ$  (Jordan et al., 1983). In this region, the onshore margin is morphotectonically segmented into the Coastal Range, the Central Valley, and the Main Cordillera (Figs. 1, 2C). Several rivers cross the low-gradient Central Valley, and cut through the Coastal Range (Fig. 1E, 2C, Table A1). Between  $39$  and  $43^\circ\text{S}$ , the transition between the Andean erosional zone and the Central Valley transfer zone features numerous large, moraine-dammed lakes in oversteepened former glacial valleys (Bentley, 1997). Central Valley sediment fill predates the LGM: depositional surfaces range in age from  $4.4 \pm 0.5$  to  $0.8 \pm 0.3$  Myr derived from K–Ar dating of intercalated lavas (Suárez and Emparan, 1997). Exposure ages of river terraces coincide with periods of low sea level (280–240 kyr and 175–135 kyr, Rehak et al., 2010). Hence, the Central Valley has experienced fluvial incision since  $\sim 0.8$  Myr, with intervening river aggradation during glacial stages and sea-level lowstands. The shelf is  $\sim 65$  km wide. The upper continental slope is smooth

and inclined at  $2$ – $4^\circ$  to a water depth of 2 km (Figs. 1, 2C). Below, the slope has steep segments alternating with slope basins, a morphology caused by continuous deformation of the accretionary prism (Völker et al., 2014). Core 50SL is located at a water depth of 4000 m within the trench on top of a debris block (200 m high) and 105 km west of the shoreline (Fig. 1D, Völker et al., 2008; Geersen et al., 2011). Sediment sources are most likely the Imperial and Tolten rivers through the Imperial/Tolten submarine canyon and subsequent northward transport in the trench as well as the Paleo-Pellahuen Canyon, which has been active during the Holocene (Bernhardt et al., 2015a). The southernmost core ODP1232 is located at 4380 m water depth 200 m west of the shore on the incoming plate and most likely receives its terrestrial sediment from the Calle-Calle, Bueno and Maullín rivers and the adjacent submarine canyons (Fig. 1E) (Blumberg et al., 2008). The Tolten, Calle-Calle, Bueno, and Maullín rivers have large piedmont lakes in their catchments (Fig. 1E). Erosion should be minimal at both core sites due to the distal location of ODP1232 and the distal and elevated position of 50SL. Cores from the continental slope were excluded from this study, as high sedimentation rates prevent the recovery of Pleistocene records (Bernhardt et al., 2015a). Due to lower onshore and offshore topographic gradients ( $11 \pm 5^\circ$  and  $4 \pm 2^\circ$ , respectively), the presence of glacial lakes along river courses, the presence of the Central Valley and a wide shelf, and the complicated dissected continental-slope morphology (Fig. 2C), we infer that the degree of connectivity is the lowest in the sediment-routing systems of Site H, when compared to Sites A and SA.

## 2.2. Climate

The SHWW govern the precipitation pattern along the Chile margin (Garreaud, 2007). At present, the margin is characterized by a strong latitudinal precipitation gradient over >2000 km from

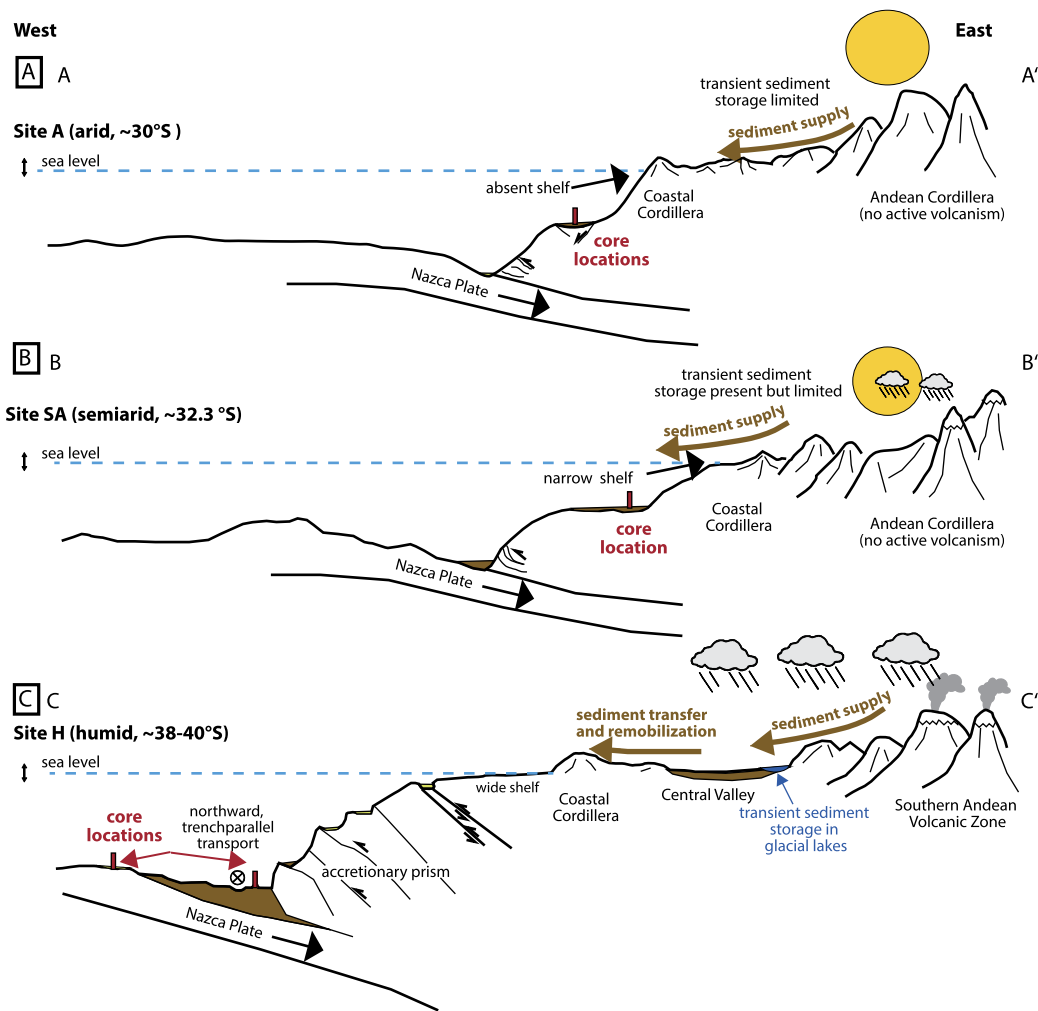


**Fig. 2.** Schematic profiles illustrating the geomorphic differences of the hinterland gradients, shelf width, and the continental slope of the three study sites (A–C). See Fig. 1 for location of study sites.

**Table 1**

Site information for the turbidite sediment cores used in this study.

Core	Latitude	Longitude	Water depth (m)	Sediment recovery (m)	Cruise	Age range (ka cal BP)	References
<b>Site A</b>							
GeoB 7136-2	−29.7167	−72.0662	3188	7.4	SO 156	2.6–26.0	Bernhardt et al. (2015a)
GeoB 7138-2	−30.1332	−71.8688	2733	6.4	SO 156	0–53.5	Bernhardt et al. (2015a)
GeoB 3368-2	−30.3600	−71.9583	3238	4.6	SO 102	0–48.7	Bernhardt et al. (2015a)
GeoB 3369-1	−30.0433	−72.0167	3457	5.5	SO 102	0–36.5	Bernhardt et al. (2015a)
<b>Site SA</b>							
GeoB 3304-5	−32.8900	−72.1917	2411	9.1	SO 102	0–24.9	Bernhardt et al. (2015a)
<b>Site H</b>							
SL 50	−38.3125	−74.6975	4380	9.1	SO 161	0.35–23.2	Blumberg et al. (2008)
ODP 1232	−39.8908	−75.9013	3187	470.0	Ocean Drilling Program Leg 202	0–141.3	Blumberg et al. (2008)

the hyperarid Atacama Desert, semiarid climate with winter rain in the central part, to year-round humid in the south (Fig. 1A). Between 18 and 33°S, the Andes are located in the subtropical belt of deserts with little to no precipitation on the western side of the mountain range. To the south, the SHWW provide abundant moisture that is forced out at the western Andean slopes, resulting in a strong increase in mean annual precipitation between 28°S to 35°S (Fig. 1A).

Millennial-scale changes in the positioning of the SHWW and precipitation patterns are well-documented along the Chile margin

in terrestrial (e.g., Veit, 1996; Valero-Garcés et al., 2005; Maldonado and Villagran, 2006) and marine archives (Lamy et al., 1999; Kim et al., 2002; Stuut and Lamy, 2004; Kaiser et al., 2005, 2008). These changes are interpreted to reflect a northward shift of the onshore precipitation pattern caused by the northward migration of the SHHW by ~5° of latitude during the LGM (e.g., Veit, 1996; Jenny et al., 2002b; Heusser et al., 2006a, 2006b; Hebbeln et al., 2007; Kaiser et al., 2008). Increased humidity during the LGM and subsequent aridification during the deglacial and the Holocene is reflected by a decrease in terrigenous sedimentation rates along

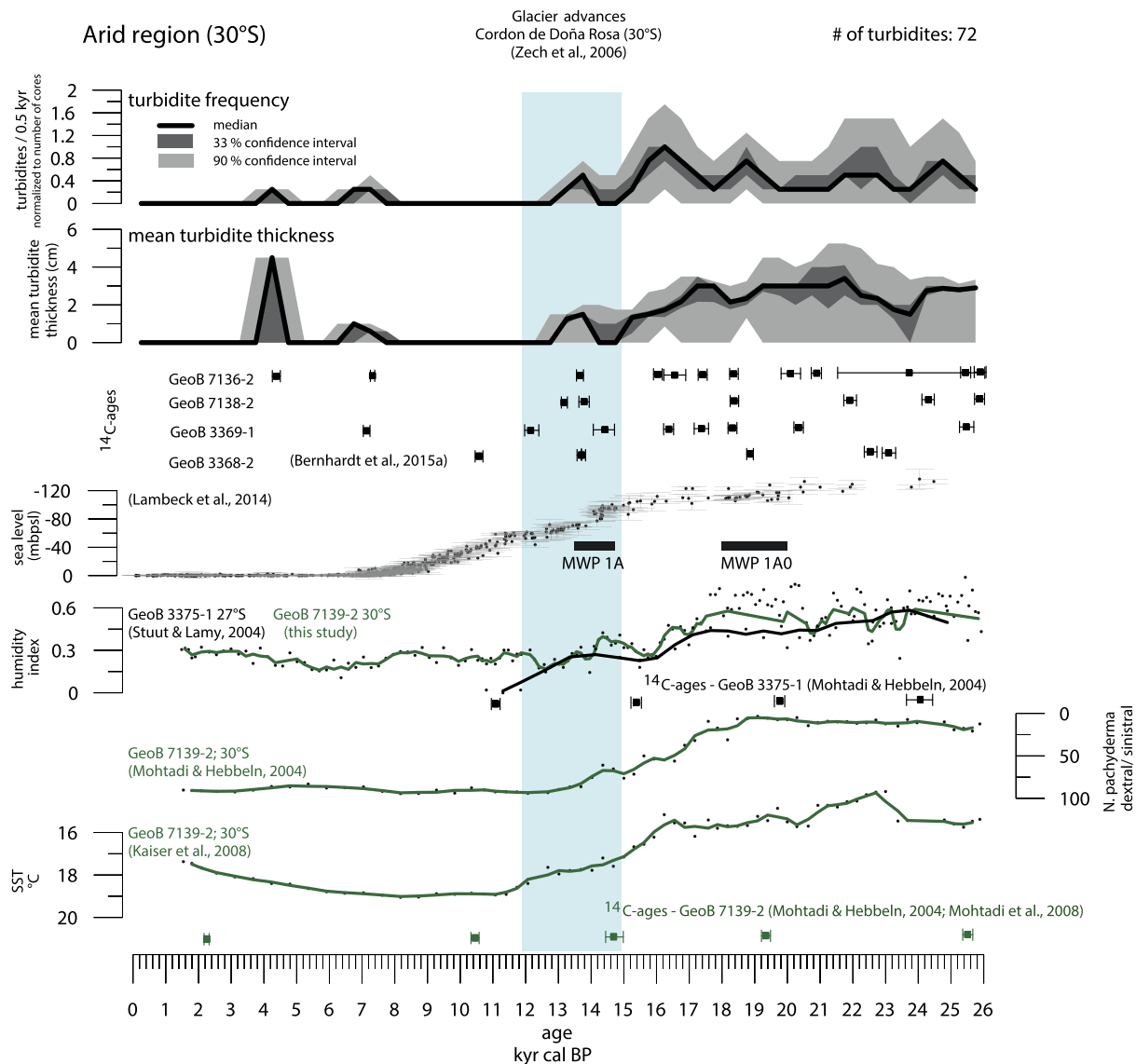


**Fig. 3.** Comparison of the turbidite records of the Site A to eustatic sea level and regional paleoclimate proxies. Note that the y-axis of sea level is inverted. For all proxies but sea level, solid lines represent 3-point moving averages. Turbidite frequency was normalized to the number of cores (4). MWP = meltwater pulse. Proxy records and  $^{14}\text{C}$ -ages are compiled from this study, Bernhardt et al., 2015a; Kaiser et al., 2008; Lambeck et al., 2014; Mohtadi and Hebbeln, 2004; Mohtadi et al., 2008; Stuut and Lamy, 2004; and Zech et al., 2006.

the continental slope from the LGM to the Holocene (Hebbeln et al., 2007).

### 3. Methods and data

#### 3.1. Age models, uncertainties and quantification of the turbidite record

Age models of turbidite cores are based on published radiocarbon ( $^{14}\text{C}$ ) ages by Blumberg et al. (2008) and Bernhardt et al. (2015a) (Figs. 3–5) and were derived using the Bayesian age-depth modeling software program BACON (Blaauw and Christen, 2011) and the Marine13-calibration curve (Reimer et al., 2013). As high sedimentation rates ( $>5$  m/kyr) hamper the recovery of Pleistocene slope records at Site H by gravity coring (Bernhardt et al., 2015a, 2016), two distal core sites in the subduction trench (SL50) and on the incoming plate (ODP1232) were included (Blumberg et al., 2008). Turbidite layers were subtracted from core depths during age-model computation. Age models of all proxy cores were recomputed using the same principles (Figs. 3–5).

At sites A and SA, ages were corrected for a reservoir-age deviation of  $\Delta R 400 \pm 100$  yrs (0–6 kyr) and  $\Delta R 31 \pm 156$  yrs ( $>6$  kyr) following Carré et al. (2016). Late Pleistocene estimates of  $\Delta R$  lack in this region. At site H, we applied an increase in  $\Delta R$  from  $400 \pm 100$  yr at ages  $<11$  kyr,  $600 \pm 200$  yr between 11 and 23 kyr, and  $800 \pm 300$  yr at ages  $>23$  kyr, acknowledging the reconstruction of  $\Delta R$  variations in the region (Siani et al., 2013). Appendix B contains the age models and their parameters for each core.

Hemipelagic and turbiditic mud can be distinguished by color differences (Blumberg et al., 2008, their Fig. 3; Bernhardt et al., 2015a, 2015b). Turbidites logged in gravity cores and ODP1232 mostly show flat and rarely irregular basal contacts, suggesting a lack of pronounced erosion (Bernhardt et al., 2015a, 2015b; Blumberg et al., 2008). However, erosional features with longer length scales than the core diameter (ODP core: 6.2 cm, gravity cores: 12 cm) cannot be identified, and we cannot exclude stratigraphic hiatuses in the turbidite record due to subsequent erosion with certainty.

Thickness measurements of turbidite layers were conducted during core description and verified using magnetic susceptibility

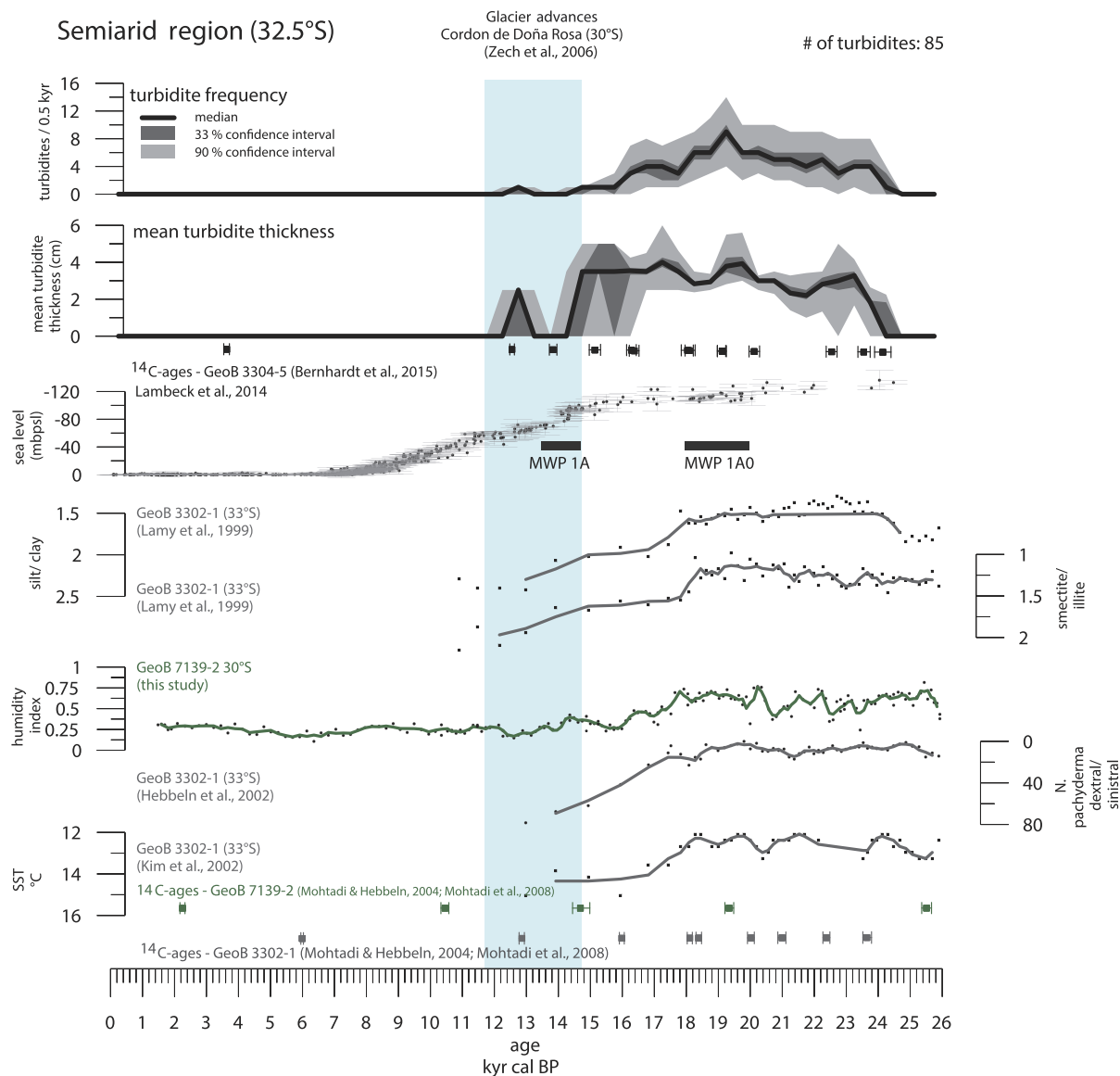


**Fig. 4.** Comparison of the turbidite records of Site SA to eustatic sea level and regional paleoclimate proxies. Note that the y-axis of sea level is inverted. For all proxies but sea level, solid lines represent 3-point moving averages. For comparison, the humidity index of Site A is also shown (GeoB7139-2 at 30°S). MWP = meltwater pulse. Proxy records and  $^{14}\text{C}$ -ages are compiled from this study, Bernhardt et al., 2015a; Hebbeln et al., 2002; Kim et al., 2002; Lambeck et al., 2014; Lamy et al., 1999; Mohtadi and Hebbeln, 2004; Mohtadi et al., 2008; and Zech et al., 2006.

measurements in Sites A and SA cores and taken from the literature for Site H (Blumberg et al., 2008). The timing of turbidite deposition is not modeled directly since turbidite layers are excluded from age-depth modeling. We thus consistently assigned the age of the directly overlying 5 mm-core slice to each turbidite layer, repeatedly for all Markov Chain Monte Carlo (MCMC) iterations returned by BACON. These ages were binned into 0.5 kyr intervals, again for all MCMC iterations, which allowed us to report the median, the 33% and 90% credibility intervals of the turbidite thickness-age and frequency-age distributions (Fig. 3–5). For the ease of intersite comparison, mean turbidite thickness per bin is plotted and turbidite frequency was normalized to the number of cores used.

The turbidite records are compared to several paleoclimate proxies (Table 2; Figs. 3–6). To analyze lag times between the turbidite record and proxies during post-LGM climate change, we compare the timing of the proxy-curve gradient change (Fig. 6). Prior to analysis, we averaged all data into 0.5 kyr bins, linearly interpolated missing data and smoothed them using a five-point

Gaussian filter with 0.5 kyr standard deviation. Subsequently, the numerical gradient of each MCMC iteration curve was calculated by central differencing and the timing of the gradient's maximum absolute value was determined, resulting in several thousand estimates for each record (black dots, Fig. 6). We also determined the duration of proxy change around these maxima by deriving the time span during which no change in gradient sign occurs (grey lines, Fig. 6).

### 3.2. Paleoclimate proxies

Cyclic climate changes and systematic Milankovitch-band cyclicity are widely recognized in (hemi-)pelagic sediments, where cyclicity is controlled by the direct influence of climate changes on the depositional environment with negligible effect of the interposed sediment-routing systems: Cyclicity is manifested, for example, in variations of planktonic organisms (Beaufort et al., 1997), wind-blown dust (e.g., Stuut and Lamy, 2004), chemical composition of organic compounds (e.g., Cacho et al., 2002), and

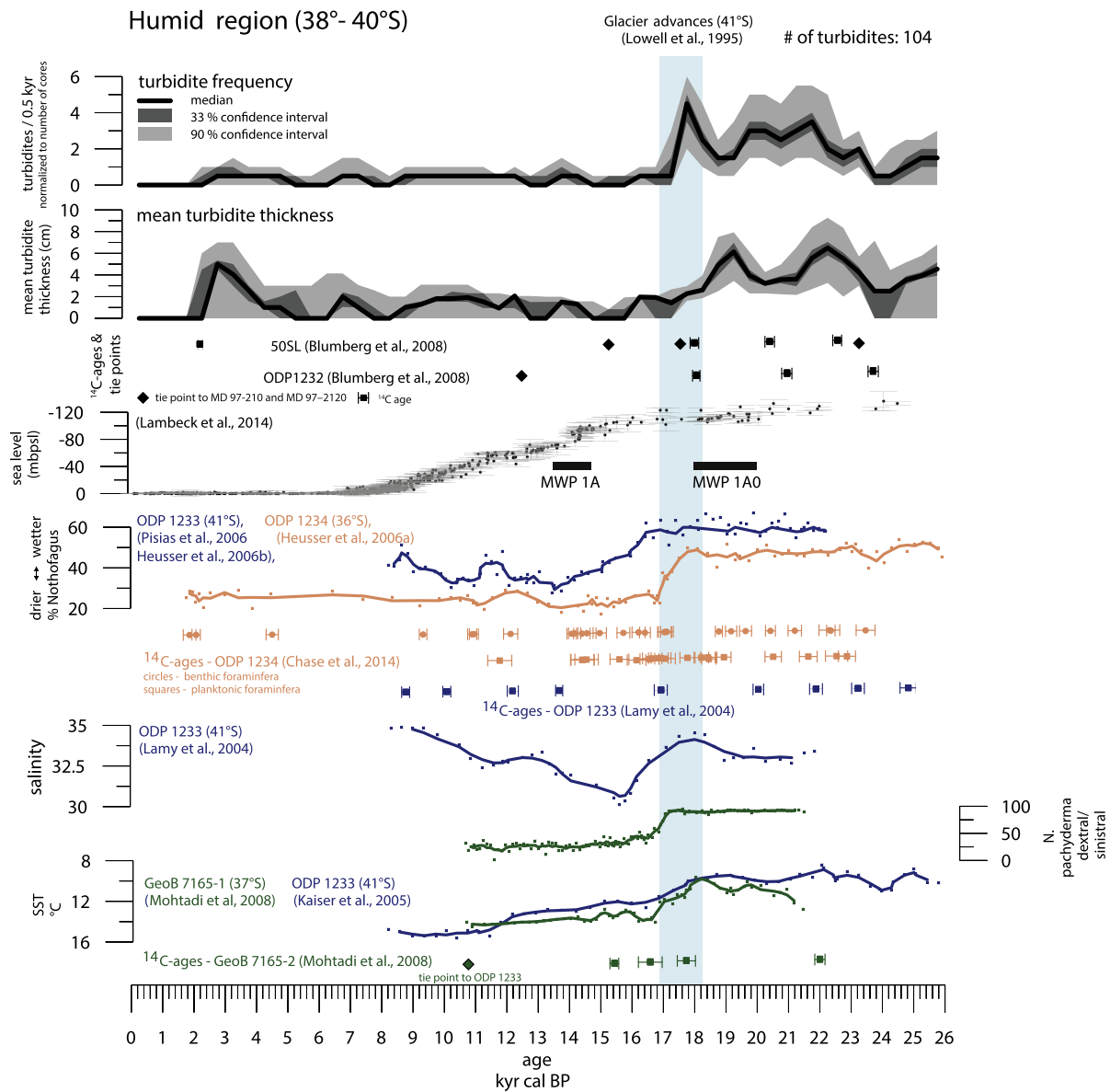


**Fig. 5.** Comparison of the turbidite records of Site H to eustatic sea level and regional paleoclimate proxies. Note that the y-axis of sea level is inverted. For all proxies but sea level, solid lines represent 3-point moving averages. Turbidite thickness and frequency were normalized to the number of cores (2). MWP = meltwater pulse. Proxy records and  $^{14}\text{C}$ -ages are compiled from this study, Blumberg et al., 2008; Chase et al., 2014; Heusser et al., 2006a, 2006b; Kaiser et al., 2005; Lambeck et al., 2014; Lowell et al., 1995; Lamy et al., 2004; Mohtadi et al., 2008; and Piasias et al., 2006.

$\delta^{18}\text{O}$ -isotopes (Imbrie et al., 1984). We refer to these proxies as ‘independent proxies’ with reference to their independence of the intermittent fluvial sediment-routing system. ‘Dependent proxies’, in contrast, are those proxies in hemipelagic sediments that, at least partly, derive from fluvial transport and are thus modulated by the efficacy of the sediment-routing system (such as detrital silts and clays, clay mineralogy, and major and trace element abundance, Table 2).

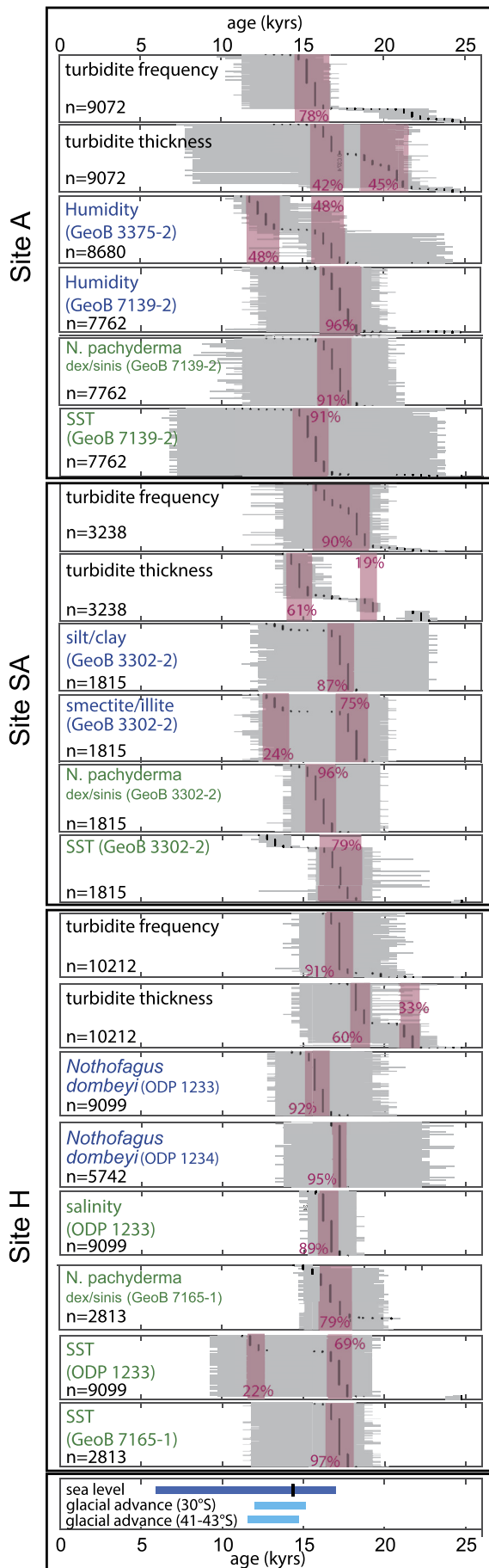
We chose the global eustatic sea-level curve of Lambeck et al. (2014) for comparison as it combines available records from the Pacific and Atlantic; however, comparisons to other curves (e.g., Siddall et al., 2003; Bintanja et al., 2005; Arz et al., 2007; Bard et al., 2010) yielded similar results. Local or regional sea-level curves over the timescale of interest are not available for the region.

The turbidite record of each site was compared to paleoclimate proxies obtained from similar latitudes to minimize the effect of possible lag times due to asynchronous north-south climatic

changes. We use a multi-proxy approach to increase the confidence of the timing of paleoclimatic changes onshore. As proxies for on-shore moisture supply and continental humidity, we used the humidity index based on grain-size end-member modeling, grain-size variations, pollen records, and clay-mineral composition of marine strata (Table 2 and references therein), all of these being dependent proxies. In addition, independent proxies for sea-surface temperatures (SST), seawater salinity, changes in paleoceanographic conditions and glacier advances constrain the timing and the manner of deglacial environmental change (Table 2). Regional, terrestrial records from lacustrine archives were excluded as they cover the Holocene only (Jenny et al., 2002a, 2002b) or lack absolute age control during the deglacial (Valero-Garcés et al., 2005). We included an additional humidity-index record based on grain-size end-member modeling (Weltje, 1997) of core GeoB7139-2 (detailed methods and interpretation in appendix A). Finally, we included records of glacial advances in the Andes around 31°S

**Table 2**  
Paleoenvironmental proxies utilized for statistical comparison with the turbidite record.

Proxy	Material & methods	Dependent/ independent	Interpretation	Sites	References
Humidity index	Grain-size distribution of the terrigenous sediment fraction in hemipelagic sediment deconvolved into subpopulations using end-member modeling	Dependent: fluvial grain-size fraction depends on terrestrial sediment routing	Grain-size distributions of deep-sea sediments were unmixed into a fluvial and an aeolian subpopulation using an end-member algorithm. The ratio of fluvial and aeolian subpopulations is used as a humidity index (the higher the more humid the terrestrial paleo-climate).	GeoB3375-1 (27°S) GeoB7139-2 (30°S)	Stuut and Lamy (2004) (this study)
Pollen	Pollen: <i>Nothofagus dombeyi</i>	Dependent proxy in the marine sediment because pollen may be transported to the ocean by fluvial systems	Decline of <i>N. dombeyi</i> : Valdivian evergreen rainforest (dominated by <i>N. dombeyi</i> ) were disrupted during the deglacial transition and subsequently gave way to the expansion of a Valdivian-Lowland deciduous forest. A decline of <i>N. dombeyi</i> pollen dominance is interpreted as a decrease in moisture supply.	ODP1234 (36°S) ODP1233 (41°S)	Pisias et al. (2006); Heusser et al. (2006a, 2006b)
Clay-mineral composition	X-ray diffraction to determine the relative percentages of chlorite smectite, and illite	Dependent on fluvial transport of clay minerals to the ocean	Illite and chlorite: mainly derived from crystalline and metamorphic rocks of the Coastal Range. Enhanced smectite contents imply increased input of sediment from volcanic Andean source rocks. Periods during which clay mineral assemblages indicate the highest influence of Andean source rocks are accompanied with low sedimentation rates. This can be explained by reduced rainfall. Modern precipitation patterns show that Andean rainfall is significantly higher than in the Coastal Range. Therefore, high smectite content (Andean source rock signal) is interpreted to indicate drier climatic intervals, whereas high chlorite and illite content (Coastal Cordillera source signal) indicate more humid conditions.	GeoB3302-1 (33°S)	Lamy et al. (1999)
Grain size	Silt and clay abundances by wet sieving and settling procedures	Dependent on fluvial transport of terrestrial detritus to the ocean	Grain-size data of terrigenous hemipelagic sediments were used as proxies for continental weathering conditions, which strongly depend on the climate. Intervals of more intense chemical weathering are interpreted to lead to finer grain sizes. Correspondingly, coarser grain sizes are characteristic of relatively reduced chemical weathering. The chemical weathering intensity in subtropical to temperate climates, as in mid-latitude Chile, is mainly determined by the amount of rainfall.	GeoB3302-1 (33°S)	Lamy et al. (1999)
Salinity	Alkenone-based sea surface temperatures (SST), $\delta^{18}\text{O}$ on <i>G. bulloides</i>	Independent	The $\delta^{18}\text{O}$ of planktic foraminifera mainly depends on the temperature and the $\delta^{18}\text{O}$ of ambient sea water ( $\delta^{18}\text{O}_w$ ). $\delta^{18}\text{O}_w$ is linearly related to salinity. Paleosalinity can be estimated when SSTs are available. The decrease in sea-surface salinity from ~17.8 to ~15.8 kyr B.P. suggests substantial freshwater input by rapid melting of the Patagonian ice sheet.	ODP1233 (41°S)	Lamy et al. (2004)
Sea-surface temperatures (SST)	Alkenone unsaturation index measured in marine sediments by capillary gas chromatography	Independent	Alkenone-derived SSTs are interpreted to correspond to the annual average SSTs. An increase in SSTs may be partly attributed to changes in oceanic currents. The deglacial increase of SSTs is interpreted to be mainly a result of the overall deglacial ocean warming.	GeoB7139-2 (30°S) GeoB3302-1 (33°S) GeoB7165 (36°S) ODP1233 (41°S)	Kaiser et al. (2005, 2008); Kim et al. (2002); Mohtadi et al. (2008)
Foraminifera-species assemblages	Planktonic foraminifera: fraction of left-coiling <i>N. pachyderma sinistral</i> relative to right-coiling <i>N. pachyderma dextral</i>	Independent	<i>N. pachyderma sin.</i> dominates colder waters, whereas <i>N. pachyderma dex.</i> dominates warmer waters. However, in the Chilean upwelling zones, a change in dominance between the 2 species also may be driven by productivity changes ( <i>N. pachyderma sin.</i> : indicator of high (paleo)productivity and/or upwelling intensity). (e.g., Mohtadi and Hebbeln, 2004). Hence, the proxy mirrors paleoenvironmental oceanic conditions.	GeoB7139-2 (30°S) GeoB3302-1 (33°S) GeoB 7165-1 (36°S)	Mohtadi et al. (2008), Mohtadi and Hebbeln (2004)



(Zech et al., 2006) and 41–43°S (Lowell et al., 1995) dated by  $^{10}\text{Be}$  exposure dating and  $^{14}\text{C}$  (recalibrated with Intcal 2013, Reimer et al., 2013), respectively.

## 4. Results

### 4.1. The turbidite record

At Site A, four sediment cores feature 72 turbidites between 26 kyr cal (calibrated) BP and present. All ages hereafter refer to calibrated years BP unless stated otherwise. Peak turbidite frequencies (maximum 1.00 [0.25, 1.75] turbidites/kyr, numbers in brackets refer to the 95% credibility interval) occur between 26 and 15 kyr and turbidite thickness peaks between 22.75 and 16.75 (max. 4.50 [1.30, 5.25] cm). Turbidite deposition stopped between 12.75 and 12.25 kyr apart from three mid-Holocene events (Fig. 3). The onset of decrease of the two turbidite parameters is between 16.25 and 16.75 kyr (Fig. 6). The most credible time interval (78% of MCMC iterations) during which turbidite frequency declines most rapidly is rather narrow between 16.25 and 14.75 kyr, although the onset of the decline of mean turbidite thickness may have occurred as early as 22 to 21 kyr (Fig. 6).

At Site SA, 85 turbidite layers were identified in core GeoB3304-5 (25 kyr-present). Turbidite frequency peaks between 24 and 16.2 kyr (max. 9.00 [4.00, 14.00] turbidites/kyr) and thickness peaks between 23.75 and 14.75 kyr (max. 4.00 [3.00, 6.00] cm) (Fig. 4). Turbidite frequency decreases after 19 kyr whereas thickness ceases abruptly after 14.75 kyr and deposition stopped between 14.75 and 14.25 kyr except for a single turbidite ~12.75 kyr (Fig. 4). 90% of MCMC iterations suggest that turbidite frequency declined most rapidly between 18 and 15.75 kyr. Mean turbidite thickness stayed rather stable during frequency reduction. The majority of simulations (61%) suggest that turbidite thickness decreased most rapidly between 15.25 and 14.25 kyr (Fig. 6).

At Site H (36–40°S), 104 turbidites were identified in cores SL50 and ODP1232 by Blumberg et al. (2008) between 26 kyr and the present day. Turbidite frequency peaks between 21.75 and 17.75 kyr (max. 4.50 [2.00, 6.00] turbidites/kyr) and mean thickness peaks between 23.25 and 18.25 kyr (max. 6.50 [3.45, 9.28] cm) (Fig. 5). Turbidite frequency ceases abruptly with 91% of the steepest gradients between 17.25 and 16.75 kyr (Fig. 5, 6). Turbidite deposition is ongoing but suppressed during the Holocene (Fig. 5).

### 4.2. Intersite comparison of the turbidite record

At Site A, the 24–15 kyr turbidite record is characterized by low-frequency (mean 0.46 [0.03, 1.17] turbidites/kyr), thin (mean 2.43 [0.12, 3.78] cm) turbidites, whereas Site SA features more frequent (mean 4.39 [1.33, 8.33] turbidites/kyr), slightly thicker (mean 3.14 [1.58, 4.23] cm) turbidites at Site SA (32.5°S) (Fig. 7). At Site H, turbidite frequency and mean thickness show intermediate values (mean 1.81 [0.75, 3.31] turbidites/kyr; mean 3.61 [3.33, 3.75] cm). The abundant Holocene turbidite activity at Site H contrasts the contemporaneous lack of turbidites at Sites A and SA (Fig. 7). However, turbidite frequency and thickness after 15 kyr are reduced by

**Fig. 6.** Comparison of the maximum deglacial proxy-curve gradients and the timing of proxy change for the three sites. The timing of the maximum gradient (black dots) of each MCMC iteration computed during age-depth modeling is plotted. Grey thin lines represent the duration of proxy change around these maxima of each MCMC iteration by deriving the time span in which no change in gradient sign occurs. 'n' denotes the number of MCMC iterations used per plot. The timing of the maximum gradient of sea level change corresponds to meltwater pulse 1a. The  $2\sigma$ -time range of the last glacial advances is also plotted but without gradient, as these are age-dated moraines. Data sources for the paleoenvironmental proxies are given in Figs. 3–5.

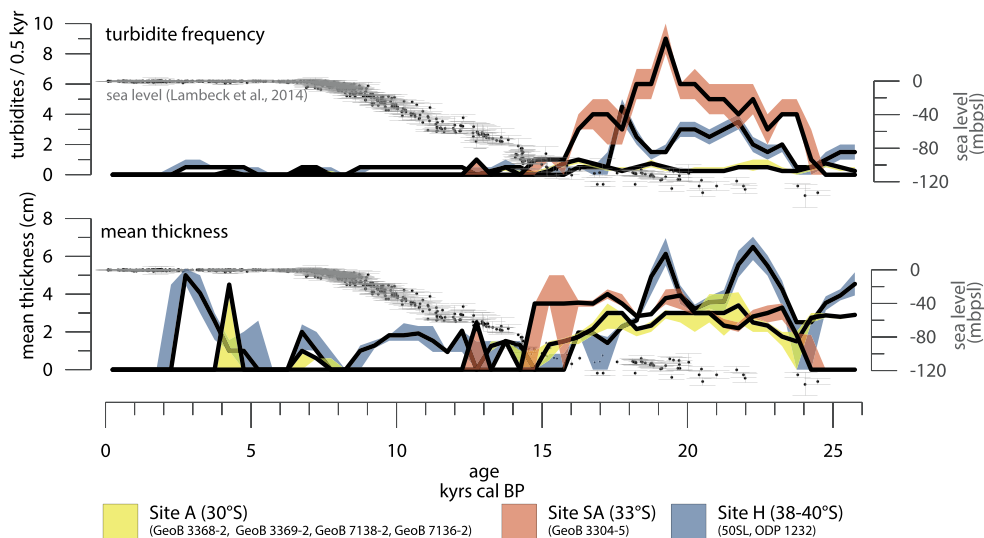


**Fig. 7.** Comparison of the turbidite-record magnitude of the three study sites (median – black curve and 33% credibility interval – colored region) in relation to the sea-level curve from Lambeck et al. (2014). Turbidite frequency was normalized to the number of cores. Data for Site H (50SL and ODP 1232) were acquired by Blumberg et al. (2008). (For interpretation of the colors in this figure, the reader is referred to the web version of this article.)

a factor 6 and 4, respectively, compared to between 24 and 15 kyr (Figs. 5, 7).

#### 4.3. Comparison of turbidite records with paleoenvironmental proxies

The onset of Holocene sea-level rise is contemporaneous with the decrease of turbidite deposition, but its maximum gradient postdates these of turbidite frequencies by up to 2 kyr (Figs. 6, 7). Paleoenvironmental proxies from the three sites indicate a pronounced regional environmental change during the deglacial (Table 2, Figs. 3–5). Moreover, the timing of independent proxy change overlaps the temporal change of dependent proxies at all three sites (Fig. 7).

The temporal range of the decline of turbidite deposition overlaps with the change of all paleoenvironmental proxies in the three study areas. At Site A, the onset of humidity decrease predates the onset of turbidite-frequency decline by up to 4 kyr. The steepest gradients of the humidity indices partly overlap with these of the turbidite-frequency curve and predate those by at most 2 kyr (Fig. 6). The decline in humidity is temporally accompanied by an increase of SSTs (91% maximum gradients: 16.25–14.75 kyr) and a change in oceanic paleoenvironmental conditions as indicated by a change in the coiling direction of planktonic foraminifera *N. pachyderma* (maximum gradient: 16–18 kyr); both independent proxies (Fig. 7). The youngest glacial advances dated from the Andean Cordillera around 30°S ( $14.7 \pm 1.5$  to  $11.6 \pm 1.2$  kyr dated by  $^{10}\text{Be}$ , hence not calibrated; Zech et al., 2006) postdate the major decline of turbidite activity, but are coeval with the termination of turbidite deposition (Fig. 3).

At Site SA, the maximum gradients of the dependent proxies (silt/clay ratio, smectite/illite content, humidity index) are contemporaneous with those of turbidite frequency, whereas the onset and steepest decline of mean turbidite thickness postdates the change indicated by independent and dependent proxies by up to 2 kyr (Figs. 4, 6). Like at Site A, deglacial environmental change, as recorded in independent proxies as the coiling direction of *N. pachyderma* and the SSTs, is coeval with the changes indicated by the dependent proxies, however, the bulk of steepest gradients for *N. pachyderma* occurs up to 2 kyr after the dependent proxies (Fig. 6). The youngest glacial advances in the Andean Cordillera at approximately 30°S are coeval with the final decline of turbidite deposition (Figs. 4, 6).

At Site H, the abrupt decrease of turbidite frequency is coeval with the steepest decrease of the dependent proxy of *Nothofagus dombeyi* pollen abundance in marine sediments of ODP 1234 (36°S), whereas the steep decline of these pollen in ODP 1233 (41°S) lag that change  $\sim 1$  kyr (Figs. 5, 6). Maximum change rates of seawater salinity, *N. pachyderma*, and SSTs as well as the final glacial advances dated from the Chilean Lake District and Isla Chiloe are contemporaneous with the decline of turbidite frequency (Fig. 5, 6). Seawater salinity shows a prominent drop of 18–16 kyr related to the melting of the Patagonian ice shield (Lamy et al., 2004).

## 5. Discussion

### 5.1. Turbidite triggers and bias of the record

Bernhardt et al. (2015a) showed that during arid conditions, even high-magnitude historic megathrust earthquakes did not trigger turbidity currents at sites A and SA. Hence, we suggest that the continental slope is relatively consolidated (ten Brink et al., 2016), and that insufficient terrestrial sediment supply suppresses considerable submarine mass wasting. During the LGM and the deglacial, turbidity currents may have been triggered by various mechanisms (earthquakes, storms, hyperpycnal discharge, submarine slope failure; Piper and Normark, 2009), which we are unable to resolve. In light of the lack of turbidites during the Holocene at sites A and SA and the timescales of interest, landslide-generated turbidity currents apparently only occur when sediment input from the continent is sufficiently high. In this context, we postulate that any potential flow trigger is restricted to loose, unconsolidated sediment rather than remobilizing older, consolidated deposits.

Compared to Site A and H, Site SA features only a single off-shore record that may be unrepresentative for the entire region as absolute values of turbidite frequency and thickness strongly depend on site location (e.g., Allin et al., 2016). The relatively low turbidite frequency and thickness in SL50 and ODP1232 may reflect their elevated and distal position above the trench floor and on the incoming plate, respectively (Figs. 1D, 7); this may represent large mass-wasting events that potentially flush canyons. However, similar depositional patterns at all study sites corroborate that the deglacial turbidite decline is a regional characteristic

rather than a significantly altered signal due to authigenic processes or other site biases.

### 5.2. Turbidite-frequency magnitude

The magnitude of turbidite frequencies partly follows the spatial pattern of long-term sediment export to the ocean that is characterized by a general north-south increase in sedimentary fill of the trench up to 41°S. The trench is largely devoid of sediment around 30°S and filled-up at 36°S (Bangs and Cande, 1997; Völker et al., 2013). Analogously, turbidite magnitudes are lowest at Site A and increase towards Site SA (Fig. 7). At Site H, lower values of turbidite frequency and thickness are likely due to more distal core locations (Figs. 1, 2). In more proximal areas, Holocene turbidite frequencies amount up to 4 turbidites/0.5 kyr in the intraslope basins at Site H (Bernhardt et al., 2016), and therefore we suggest that the late Pleistocene turbidite-record magnitude in the intraslope basins of Site H also exceeds those of Site SA.

### 5.3. Age-model resolution and lag times

The resolution of the age models determines our ability of detecting lag times between environmental forcings and the expression of these forcings in the depositional areas. However, the timing and pattern of deglacial turbidite frequency and mean thickness decline differ (e.g., Site SA, Fig. 6), and are subject to significant uncertainties as shown by the wide spread of MCMC iterations (Fig. 6). However, the most credible temporal region of the steepest gradients lies within time spans from 1–4 kyr. Hence, we infer that sediment-routing systems responded rapidly, although lag times between the turbidite record to the environmental proxies below these time ranges may occur and remain undetected.

### 5.4. Processes promoting signal propagation

The spatiotemporal patterns of turbidite activity along the Chile margin and their relation to a potential suite of forcing mechanisms allow us to infer source-to-sink dynamics at the timescale of global climate cycles. Besides few lacustrine records at Site SA (e.g., Jenny et al., 2002b; Valero-Garcés et al., 2005) and H (e.g., Heirman et al., 2011 and others), marine depocenters contain the most complete, geochronologically constrained archives that potentially capture changes along the sediment-routing systems of the western Andes. The sharp deglacial decline of turbidite deposition at all sites indicates an overall rapid response to past environmental change at millennial to possibly centennial timescales.

The steepest gradients of sea-level transgression (corresponding to Meltwater Pulse (MWP) 1a) postdate the steepest decline of turbidite deposition (Figs. 6, 7). Yet we cannot exclude that an early, slow rise in sea level (e.g., MWP 1a, ~10–15 m between 20 and 18 kyr) and flooding of critical outer shelf areas affected turbidite activity. However, we expect only minor, if any influence on turbidite activity at this site because early sea-level rise would have only affected a small portion of the partly absent and narrow shelf at Site A. Site SA features a narrow shelf, too, and onset of MWP 1a postdates the onset of decline of turbidite frequencies. Similarly, at Site H, the most rapid decline of turbidite thickness occurs before the earliest sea-level rise (MWP 1a, Fig. 5, 6). Thus, deglacial turbidite decline is unlikely to be mainly controlled by eustatic sea-level rise. Instead, onshore processes that caused decreasing sediment export to the ocean are probable controls on turbidite activity. We note, however that the sea-level curve used in this study (Lambeck et al., 2014) is a global eustatic curve and may miss local sea-level deviations (e.g., by isostatic effects). However, a local sea-level curve does not exist for the timescale of interest.

To untangle onshore processes and controls on turbidite activity, our analysis and interpretation rely on the timing of the maximum gradient of different proxy curves and the onshore geomorphic situation. At sites A and SA, dependent proxies (humidity index, silt/clay, smectite/illite) indicate increasing aridity accompanied by the warming of SSTs (independent proxy). The maximum decline of turbidite parameters occurs at the same time as the onshore return to arid conditions with no resolvable lag-times (Fig. 6). Mean turbidite thickness at Site SA lags the steepest decline of the dependent proxies by ~1 kyr, a delayed response that may be attributed to the lower connectivity of the routing system at Site SA (Fig. 1B, 2B). We argue that the erosional and/or transfer zone at Site A and SA responded rapidly to an inferred deglacial decrease in sediment production. Together with the onset of aridification and a likely reduction of sediment-transport capacity these onshore environmental changes diminished sediment supply ( $Q_s$ ) to the ocean. The topographic steepness and related lack of major sediment-storage landforms at Site A and SA suggest a highly connected sediment transport system between the topographically high Andean erosional zone and the Pacific Ocean depositional zone. A rapid sedimentary response to changes in the erosional zone thus seems plausible.

The contemporaneity of the youngest glacial advances in the Andean Cordillera at 30°S and the offshore decline of turbidites indicate that moisture supply to the Andean Cordillera was sufficient to feed glacial advances while rivers lacked the capacity to transport sufficient material to the ocean (Figs. 3, 4). However, post-LGM glaciers expanded only ~5 km from today's unglaciated cirques; a small distance compared to an earlier advance of >30 km at ~31 kyr (Zech et al., 2006). The volume of meltwater released after the last glacial advance was thus much smaller than that of previous phases, a finding supported by the lack of significant changes in the  $\delta^{18}\text{O}$  records of seawater along these latitudes (De Pol-Holz et al., 2007) and in any other proxies (Figs. 3, 4). Independent and dependent proxies show a very similar timing of the deglacial environmental changes (Fig. 6), supporting the notion that these sediment-routing systems were reactive and highly connected at that time.

The synchronous decline of turbidite deposition and humidity-proxy change in the southern, humid sediment-routing systems of site H may be due to different reasons. The Chilean Lake District hosted several piedmont glaciers during Pleistocene stadials and now comprises >15 glacial lakes between 39° and 43°S (e.g., Bentley, 1997; Fig. 1E). These lakes at the foothills of the Andes are often moraine-dammed and located in over-deepened (several 100 m) glacial valleys. Upon deglaciation, these basins may have instantaneously acted as sediment traps that decoupled the erosional zone in the Andes and the transfer zone of the Central Valley, thus leading to a sharp loss of connectivity of the sediment-routing system and a concomitant strong reduction of  $Q_s$  to the ocean. The lakes may have efficiently filtered out the coarse Andean-derived sediment fraction from the routing system, whereas they likely bypassed a fraction of the suspended load. This interpretation is consistent with ongoing, but mud-dominated (Bernhardt et al., 2015a) Holocene turbidite sedimentation on the continental slope around 37–38°S (close to site H; Bernhardt et al., 2016) as compared to sand-rich Holocene turbidite deposits on the Biobío submarine fan that lacks glacial lakes in its catchment (Bernhardt et al., 2015b).

Uncertainties, however, remain about the deglaciation history of the Lake District. Earliest signs of deglaciation are dated to 24.8–28.0 kyr (Charlet et al., 2008) and lakes became ice-free between 17.9 kyr (Sterken et al., 2008) and 14.1 kyr (Bentley, 1997). However, spatio-temporal patterns of deglaciation are non-uniform (Bentley, 1997; Heirman et al., 2011). Nevertheless, the time frame

of deglaciation for some of the lakes coincides with the decline of turbidite deposition along similar latitudes.

An alternative explanation for the marine turbidite depositional pattern at site H is related to the decreased moisture supply (as recorded in the dependent proxy of the pollen record in ODP1233 and 1234; Table 2) and the rapid propagation of its signal. Moisture decline possibly decreased erosion in the hinterland, as well as river-transport capacity through connected compartments of the sediment-routing systems. Yet, low topographic onshore and offshore gradients due to the Central Valley and the wide shelf, respectively, the presence of lakes along the river course, and the complicated dissected, structurally controlled continental slope morphology (Fig. 2) conform to a lower degree of connectivity of Site H compared to Site A and SA. However, mid-Pleistocene ages of depositional surfaces (>0.8 Ma, Suárez and Emparan, 1997) and pre-LGM establishment of river valleys (Rehak et al., 2010) indicate that the Central Valley efficiently conveys sediment to the coast. Moreover, low sea level and southwestward sediment transport on the shelf by undercurrents (Bernhardt et al., 2016) may have further increased system connectivity. Still, a certain lag time between climatic forcing and response may be expected, but remained below the temporal resolution of our records (~1 to 4 kyr).

Ocean salinity and the timing of the last glacier advance suggest that large volumes of melt water were released during or after the decline of turbidite deposition at site H (Figs. 5, 6C). However, turbidites do not mirror a sedimentary signal that shows increased  $Q_s$  due to glacial melting, suggesting that sediment was released into partly ice-free piedmont lakes. Therefore, we hypothesize that glacier retreat from some of the major glacial lakes and the accompanied sudden reduction of connectivity between the Andean erosional zone and the Central Valley transfer zone is mainly responsible for the very rapid decrease of turbidite frequencies at site H, and fluvial transport-capacity changes due to reduced precipitation played only a minor role.

## 6. Conclusions

Turbidite deposits on the continental slope and deep ocean basin preserve information on the LGM to Holocene climatic transition along the Chile continental margin (30–40°S) over a wide range of climates and geomorphic settings, an encouraging result as this allows the use of turbidite strata as valuable sedimentary archives under certain environmental circumstances. Our analysis suggests that turbidite decline is not mainly controlled by post-glacial sea-level rise. Instead, we propose that it is the interplay of distinct factors in each setting along the Chile continental margin that promotes rapid propagation of environmental changes from the hinterland into the marine depocenters. At the arid and semi-arid sites (Site A and SA), sediment-routing systems are highly connected and a deglacial return to arid conditions caused by the southward retreat of the SHWW has resulted in decreased river-transport capacity. Rivers were thus unable to remove available glacial sediments from the Andean hinterland. This is rapidly manifested in a decrease of turbidite deposition in the marine sink, generally with no resolvable lag times between the environmental proxy change and the decline in turbidite deposition.

At the southern, humid study site (Site H), the similar temporal turbidite depositional pattern is interpreted to be mainly attributed to the sudden loss of connectivity between the Andean erosional zone and the Central Valley transfer zone by the exposure of piedmont-lake basins from glacial ice. However, decreased continental humidity and related runoff may have additionally contributed to the rapid decrease in turbidite deposition. Hence, the sedimentary response to climate change archived as turbidite depositional patterns in the marine sink under contrasting connectivity scenarios can result in uniform patterns of turbidite frequency,

but may be caused by different underlying mechanisms. Our study suggests that the response time of a system, and hence the lag times between the forcing and the sedimentary record, is significantly influenced by temporal changes of connectivity between different geomorphic compartments along the sediment-routing system. Rapid changes in the connectivity of the sediment-routing system may result in rapid manifestation of a climate signal in the downstream geological archive and may, thus, create meaningful stratigraphic patterns.

## Acknowledgements

A. Bernhardt was funded by German Research Foundation (DFG) grant BE 5070/1-1. The German Federal Ministry of Education and Research (BMBF) provided financial support for R/V Sonne cruises 102, 156 and 161 (CHIPAL 03G0102A, PUCK 03G0156A, SPOC 03G0161A). Samples from GeoB cores were provided by the MARUM – Center for Marine Environmental Sciences at the University of Bremen. We thank Gert-Jan Weltje for making the end-member algorithm available. Data presented in this study are available at <https://doi.pangaea.de/10.1594/PANGAEA.876590>. Michael Clare and an anonymous reviewer provided constructive criticism that significantly improved the manuscript.

## Appendix. Supplementary material

Supplementary material related to this article can be found online at <http://dx.doi.org/10.1016/j.epsl.2017.05.017>.

## References

- Allen, P.A., 2008. Time scales of tectonic landscapes and their sediment routing systems. *Geol. Soc. (Lond.) Spec. Publ.* 296, 7–28. <http://dx.doi.org/10.1144/SP296.2>.
- Allin, J.R., Hunt, J.E., Talling, P.J., Clare, M.A., Pope, E., Masson, D.G., 2016. Different frequencies and triggers of canyon filling and flushing events in Nazare Canyon, offshore Portugal. *Mar. Geol.* 371, 89–105. <http://dx.doi.org/10.1016/j.margeo.2015.11.005>.
- Armitage, J.J., Dunkley Jones, T., Duller, R.A., Whittaker, A.C., Allen, P.A., 2013. Temporal buffering of climate-driven sediment flux cycles by transient catchment response. *Earth Planet. Sci. Lett.* 369–370, 200–210. <http://dx.doi.org/10.1016/j.epsl.2013.03.020>.
- Arz, H.W., Lamy, F., Ganopolski, A., Nowaczyk, N., Pätzold, J., 2007. Dominant Northern Hemisphere climate control over millennial-scale glacial sea-level variability. *Quat. Sci. Rev.* 26, 312–321. <http://dx.doi.org/10.1016/j.quascirev.2006.07.016>.
- Bangs, N.L., Cande, S.C., 1997. Episodic development of a convergent margin inferred from structures and processes along the southern Chile margin. *Tectonics* 16, 489–503. <http://dx.doi.org/10.1029/97TC00494>.
- Bard, E., Hamelin, B., Delanghe-Sabatier, D., 2010. Deglacial meltwater pulse 1B and Younger Dryas sea levels revisited with boreholes at Tahiti. *Science* 327, 1235–1237. <http://dx.doi.org/10.1126/science.1180557>.
- Beaufort, L., Lancelot, Y., Camberlin, P., Cayre, O., Vincent, E., Bassinot, F., Labeyrie, L., 1997. Insolation cycles as a major control of equatorial Indian Ocean primary production. *Science* 278, 1451–1454. <http://dx.doi.org/10.1126/science.278.5342.1451>.
- Bentley, M.J., 1997. Relative and radiocarbon chronology of two former glaciers in the Chilean Lake District. *J. Quat. Sci.* 12, 25–33. [http://dx.doi.org/10.1002/\(SICI\)1099-1417\(199701/02\)12:1<25::AID-JQS289>3.0.CO;2-A](http://dx.doi.org/10.1002/(SICI)1099-1417(199701/02)12:1<25::AID-JQS289>3.0.CO;2-A).
- Bernhardt, A., Hebbeln, D., Lückge, A., Melnick, D., Strecker, M.R., 2015a. Turbidite paleoseismology along the Chilean continental margin – feasible or not? *Quat. Sci. Rev.* 120, 71–92. <http://dx.doi.org/10.1016/j.quascirev.2015.04.001>.
- Bernhardt, A., Hebbeln, D., Regenberg, M., Lückge, A., Strecker, M.R., 2016. Shelfal sediment transport by an undercurrent forces turbidity current activity during high sea level, Chile continental margin. *Geology* 44, 295–298. <http://dx.doi.org/10.1130/G37594.1>.
- Bernhardt, A., Melnick, D., Jara-Muñoz, J., Argandoña, B., González, J., Strecker, M.R., 2015b. Controls on submarine canyon activity during sea-level highstands: the Biobío canyon system offshore Chile. *Geosphere* 11, 1–30. <http://dx.doi.org/10.1130/GES01063.1>.
- Bintanja, R., van de Wal, R.S.W., Oerlemans, J., 2005. Modelled atmospheric temperatures and global sea levels over the past million years. *Nature* 437, 125–128. <http://dx.doi.org/10.1038/nature03975>.
- Blaauw, M., Christen, J., 2011. Flexible paleoclimate age-depth models using an autoregressive gamma process. *Bayesian Anal.* 6, 457–474. <http://dx.doi.org/10.1214/11-BA618>.

- Blumberg, S., Lamy, F., Arz, H., Ehtler, H., Wiedicke, M., Haug, G., Oncken, O., 2008. Turbiditic trench deposits at the South-Chilean active margin: a Pleistocene–Holocene record of climate and tectonics. *Earth Planet. Sci. Lett.* 268, 526–539. <http://dx.doi.org/10.1016/j.epsl.2008.02.007>.
- Bonneau, L., Jorry, S.J., Toucanne, S., Silva Jacinto, R., Emmanuel, L., 2014. Millennial-scale response of a Western Mediterranean River to late Quaternary climate changes: a view from the deep sea. *J. Geol.* 122, 687–703. <http://dx.doi.org/10.1086/677844>.
- Bracken, L.J., Turnbull, L., Wainwright, J., Bogaart, P., 2015. Sediment connectivity: a framework for understanding sediment transfer at multiple scales. *Earth Surf. Process. Landf.* 40, 177–188. <http://dx.doi.org/10.1002/esp.3635>.
- Braun, J., Voisin, C., Gourlan, A.T., Chauvel, C., 2015. Erosional response of an actively uplifting mountain belt to cyclic rainfall variations. *Earth Surf. Dyn.*, 1–14. <http://dx.doi.org/10.5194/esurf-3-1-2015>.
- Brierley, G., Fryirs, K., Jain, V., 2006. Landscape connectivity: the geographic basis of geomorphic applications. *Area* 38, 165–174. <http://dx.doi.org/10.1111/j.1475-4762.2006.00671.x>.
- Brunsdon, D., Thornes, J.B., 1979. Landscape sensitivity and change. *Trans. Inst. Br. Geogr.* 4, 463–484.
- Cacho, I., Grimalt, J.O., Canals, M., 2002. Response of the Western Mediterranean Sea to rapid climatic variability during the last 50,000 years: a molecular biomarker approach. *J. Mar. Syst.* 34, 253–272.
- Carré, M., Jackson, D., Maldonado, A., Chase, B.M., Sachs, J.P., 2016. Variability of <sup>14</sup>C reservoir age and air–sea flux of CO<sub>2</sub> in the Peru–Chile upwelling region during the past 12,000 years. *Quat. Res. (United States)* 85, 87–93. <http://dx.doi.org/10.1016/j.yqres.2015.12.002>.
- Carter, L., Gavey, R., Talling, P.J., Liu, J.T., 2014. Insights into submarine geohazards from breaks in subsea telecommunication cables. *Oceanography* 24, 58–67. <http://dx.doi.org/10.5670/oceanog.2011.65>.
- Castelltort, S., Whittaker, A., Vergés, J., 2015. Tectonics, sedimentation and surface processes: from the erosional engine to basin deposition. *Earth Surf. Process. Landf.* 40, 1839–1846. <http://dx.doi.org/10.1002/esp.3769>.
- Charlet, F., De Batist, M., Chapron, E., Bertrand, S., Pino, M., Urrutia, R., 2008. Seismic stratigraphy of Lago Puyehue (Chilean Lake District): new views on its deglacial and Holocene evolution. *J. Paleolimnol.* 39, 163–177. <http://dx.doi.org/10.1007/s10933-007-9112-3>.
- Chase, Z., McManus, J., Mix, A.C., Muratli, J., 2014. Southern-ocean and glaciogenic nutrients control diatom export production on the Chile margin. *Quat. Sci. Rev.* 99, 135–145. <http://dx.doi.org/10.1016/j.quascirev.2014.06.015>.
- Clare, M.A., Talling, P.J., Hunt, J.E., 2015. Implications of reduced turbidity current and landslide activity for the Initial Eocene Thermal Maximum – evidence from two distal, deep-water sites. *Earth Planet. Sci. Lett.* 420, 102–115. <http://dx.doi.org/10.1016/j.epsl.2015.03.022>.
- Clift, P.D., Giosan, L., 2014. Sediment fluxes and buffering in the post-glacial Indus Basin. *Basin Res.* 26, 369–386. <http://dx.doi.org/10.1111/bre.12038>.
- Contreras-Reyes, E., Ruiz, J.A., Becerra, J., Kopp, H., Reichert, C., Maksymowicz, A., Arriagada, C., 2015. Structure and tectonics of the central Chilean margin (31°–33°S): implications for subduction erosion and shallow crustal seismicity. *Geophys. J. Int.* 203, 776–791. <http://dx.doi.org/10.1093/gji/ggv309>.
- Coulthard, T.J., Van De Wiel, M.J., 2013. Climate, tectonics or morphology: what signals can we see in drainage basin sediment yields? *Earth Surf. Dyn.* 1, 13–27. <http://dx.doi.org/10.5194/esurf-1-13-2013>.
- Covault, J.A., Graham, S.A., 2010. Submarine fans at all sea-level stands: tectono-morphologic and climatic controls on terrigenous sediment delivery to the deep sea. *Geology* 38, 939–942. <http://dx.doi.org/10.1130/G31081.1>.
- Covault, J.A., Normark, W.R., Romans, B.W., Graham, S.A., 2007. Highstand fans in the California borderland: the overlooked deep-water depositional systems. *Geology* 35, 783–786. <http://dx.doi.org/10.1130/G23800A.1>.
- Covault, J.A., Romans, B.W., Fildani, A., McGann, M., Graham, S.A., 2010. Rapid climatic signal propagation from source to sink in a Southern California sediment-routing system. *J. Geol.* 118, 247–259. <http://dx.doi.org/10.1086/651539>.
- De Pol-Holz, R., Ulloa, O., Lamy, F., Dezileau, L., Sabatier, P., Hebbeln, D., 2007. Late Quaternary variability of sedimentary nitrogen isotopes in the eastern South Pacific Ocean. *Paleoceanography* 22, 1–16. <http://dx.doi.org/10.1029/2006PA001308>.
- Denton, G.H., Heusser, C.J., Lowell, T.V., Moreno, P.L., Andersen, B.G., Heusser, L.E., Schluchter, C., Marchant, D.R., 1999. Interhemispheric linkage of paleoclimate during the last Glaciation. *Geogr. Ann. Ser. A Phys. Geogr.* 81, 107. <http://dx.doi.org/10.1111/j.0435-3676.1999.00055.x>.
- Ducassou, E., Migeon, S., Mulder, T., Murat, A., Capotondi, L., Bernasconi, S.M., Mascle, J., 2009. Evolution of the Nile deep-sea turbidite system during the Late Quaternary: influence of climate change on fan sedimentation. *Sedimentology* 56, 2061–2090. <http://dx.doi.org/10.1111/j.1365-3091.2009.01070.x>.
- Galy, V., France-Lanord, C., Beyssac, O., Faure, P., Kudrass, H., Palhol, F., 2007. Efficient organic carbon burial in the Bengal fan sustained by the Himalayan erosional system. *Nature* 450, 407–410. <http://dx.doi.org/10.1038/nature06273>.
- Garcin, Y., Schildgen, T.F., Torres, V., Melnick, D., Guillemoteau, J., Willenbring, J., Strecker, M.R., 2017. Short-lived increase in erosion during the African Humid Period: evidence from the northern Kenya Rift. *Earth Planet. Sci. Lett.* 459, 58–69. <http://dx.doi.org/10.1016/j.epsl.2016.11.017>.
- Garreaud, R., 2007. Precipitation and circulation covariability in the extratropics. *J. Climate* 20, 4789–4797. <http://dx.doi.org/10.1175/JCLI4257.1>.
- Geersen, J., Völker, D., Behrmann, J.H., Reichert, C., Krastel, S., 2011. Pleistocene giant slope failures offshore Arauco Peninsula, Southern Chile. *J. Geol. Soc. Lond.* 168, 1237–1248. <http://dx.doi.org/10.1144/0016-76492011-027>.
- Godard, V., Tucker, G.E., Burch Fisher, G., Burbank, D.W., Bookhagen, B., 2013. Frequency-dependent landscape response to climatic forcing. *Geophys. Res. Lett.* 40, 859–863. <http://dx.doi.org/10.1002/grl.50253>.
- Hebbeln, D., Marchant, M., Wefer, G., 2002. Paleoproductivity in the southern Peru–Chile Current through the last 33,000 yr. *Mar. Geol.* 186, 487–504. [http://dx.doi.org/10.1016/S0025-3227\(02\)00331-6](http://dx.doi.org/10.1016/S0025-3227(02)00331-6).
- Hebbeln, D., Lamy, F., Mohtadi, M., Ehtler, H.P., 2007. Tracing the impact of glacial–interglacial climate variability on erosion of the southern Andes. *Geology* 35, 131–134. <http://dx.doi.org/10.1130/G23243A.1>.
- Heckmann, T., Schwanghart, W., 2013. Geomorphic coupling and sediment connectivity in an alpine catchment – exploring sediment cascades using graph theory. *Geomorphology* 182, 89–103. <http://dx.doi.org/10.1016/j.geomorph.2012.10.033>.
- Heirman, K., De Batist, M., Charlet, F., Moernaut, J., Chapron, E., Bruemmer, R., Pino, M., Urrutia, R., 2011. Detailed seismic stratigraphy of Lago Puyehue: implications for the mode and timing of glacier retreat in the Chilean Lake District. *J. Quat. Sci.* 26, 665–674. <http://dx.doi.org/10.1002/jqs.1491>.
- Heusser, L., Heusser, C., Mix, A., McManus, J., 2006a. Chilean and Southeast Pacific paleoclimate variations during the last glacial cycle: directly correlated pollen and  $\delta^{18}\text{O}$  records from ODP Site 1234. *Quat. Sci. Rev.* 25, 3404–3415. <http://dx.doi.org/10.1016/j.quascirev.2006.03.011>.
- Heusser, L., Heusser, C., Pisias, N., 2006b. Vegetation and climate dynamics of southern Chile during the past 50,000 years: results of ODP Site 1233 pollen analysis. *Quat. Sci. Rev.* 25, 474–485. <http://dx.doi.org/10.1016/j.quascirev.2005.04.009>.
- Hinderer, M., 2012. From gullies to mountain belts: a review of sediment budgets at various scales. *Sediment. Geol.* 280, 21–59. <http://dx.doi.org/10.1016/j.sedgeo.2012.03.009>.
- Hoffmann, T., 2015. Sediment residence time and connectivity in non-equilibrium and transient geomorphic systems. *Earth-Sci. Rev.* 150, 609–627. <http://dx.doi.org/10.1016/j.earscirev.2015.07.008>.
- Imbrie, J., Hays, J.D., Martinson, D.G., McIntyre, A., Mix, A.C., Morley, J.J., Pisias, N.G., Prell, W.L., Shackleton, N.J., 1984. The orbital theory of Pleistocene climate: support from a revised chronology of the marine  $\delta^{18}\text{O}$  record. In: Berger, A., Imbrie, J., Hays, H., Kukla, G.B.S. (Eds.), *Milankovitch and Climate: Understanding the Response to Astronomical Forcing*, Proceedings of the NATO Advanced Research Workshop Held 30 November–4 December, 1982 in Palisades, NY. D. Reidel Publishing, Dordrecht, p. 269.
- Jain, V., Tandon, S.K., 2010. Conceptual assessment of (dis)connectivity and its application to the Ganga River dispersal system. *Geomorphology* 118, 349–358. <http://dx.doi.org/10.1016/j.geomorph.2010.02.002>.
- Jenny, B., Valero-Garcés, B.L., Urrutia, R., Kelts, K., Veit, H., Appleby, P.G., Geyh, M., 2002a. Moisture changes and fluctuations of the Westerlies in Mediterranean Central Chile during the last 2000 years: the Laguna Aculeo record (33°50'S). *Quat. Int.* 87, 3–18. [http://dx.doi.org/10.1016/S1040-6182\(01\)00058-1](http://dx.doi.org/10.1016/S1040-6182(01)00058-1).
- Jenny, B., Valero-Garcés, B.L., Villa-Martinez, R., Urrutia, R., Geyh, M., Veit, H., 2002b. Early to mid-Holocene aridity in central Chile and the southern Westerlies: the Laguna Aculeo record (34°S). *Quat. Res.* 58, 160–170. <http://dx.doi.org/10.1006/qres.2002.2370>.
- Jerolmack, D.J., Paola, C., 2010. Shredding of environmental signals by sediment transport. *Geophys. Res. Lett.* 37, 1–5. <http://dx.doi.org/10.1029/2010GL044638>.
- Jordan, T.E., Isacks, B.L., Allmendinger, R.W., Brewer, J.A., Ramos, V.A., Ando, C.J., 1983. Andean tectonics related to geometry of subducted Nazca plate. *Geol. Soc. Am. Bull.* 94, 341–361. [http://dx.doi.org/10.1130/0016-7606\(1983\)94<341:ATRTGO>2.0.CO;2](http://dx.doi.org/10.1130/0016-7606(1983)94<341:ATRTGO>2.0.CO;2).
- Kaiser, J., Lamy, F., Hebbeln, D., 2005. A 70-kyr sea surface temperature record off southern Chile (Ocean Drilling Program Site 1233). *Paleoceanography* 20, 1–15. <http://dx.doi.org/10.1029/2005PA001146>.
- Kaiser, J., Schefus, E., Lamy, F., Mohtadi, M., Hebbeln, D., 2008. Glacial to Holocene changes in sea surface temperature and coastal vegetation in north central Chile: high versus low latitude forcing. *Quat. Sci. Rev.* 27, 2064–2075. <http://dx.doi.org/10.1016/j.quascirev.2008.08.025>.
- Kim, J., Schneider, R., Hebbeln, D., 2002. Last deglacial sea-surface temperature evolution in the Southeast Pacific compared to climate changes on the South American continent. *Quat. Sci.* 21, 2085–2097.
- Lambeck, K., Rouby, H., Purcell, A., Sun, Y., Sambridge, M., 2014. Sea level and global ice volumes from the Last Glacial Maximum to the Holocene. *Proc. Natl. Acad. Sci. USA* 111, 15296–15303. <http://dx.doi.org/10.1073/pnas.1411762111>.
- Lamy, F., Hebbeln, D., Wefer, G., 1999. High-resolution marine record of climatic change in mid-latitude Chile during the last 28,000 years based on terrigenous sediment parameters. *Quat. Res.* 51, 83–93. <http://dx.doi.org/10.1006/qres.1998.2010>.
- Lamy, F., Kaiser, J., Ninnemann, U., Hebbeln, D., Arz, H.W., Stoner, J., 2004. Antarctic timing of surface water changes off Chile and Patagonian ice sheet response. *Science* 304, 1959–1962. <http://dx.doi.org/10.1126/science.1097863>.
- Laursen, J., Normark, W.R., 2002. Late Quaternary evolution of the San Antonio Submarine Canyon in the central Chile forearc (~33°S). *Mar. Geol.* 188, 365–390. [http://dx.doi.org/10.1016/S0025-3227\(02\)00421-8](http://dx.doi.org/10.1016/S0025-3227(02)00421-8).

- Laursen, J., Normark, W.R., 2003. Impact of structural and autocyclic basin-floor topography on the depositional evolution of the deep-water Valparaíso forearc basin, central Chile. *Basin Res.* 15, 201–226. <http://dx.doi.org/10.1046/j.1365-2117.2003.00205.x>.
- Lowell, T.V., Heusser, C.J., Andersen, B.G., Moreno, P.I., Hauser, A., Heusser, L.E., Schlüchter, C., Marchant, D.R., Denton, G.H., 1995. Interhemispheric correlation of late pleistocene glacial events. *Science* 269, 1541–1549. <http://dx.doi.org/10.1126/science.269.5230.1541>.
- Maldonado, A., Villagran, C., 2006. Climate variability over the last 9900 cal yr BP from a swamp forest pollen record along the semiarid coast of Chile. *Quat. Res.* 66, 246–258. <http://dx.doi.org/10.1016/j.yqres.2006.04.003>.
- Métivier, F., Gaudemer, Y., 1999. Stability of output fluxes of large rivers in South and East Asia during the last 2 million years: implications on floodplain processes. *Basin Res.* 11, 293–304.
- Mohtadi, M., Hebbeln, D., 2004. Mechanisms and variations of the paleoproductivity off northern Chile (24°S–33°S) during the last 40,000 years. *Paleoceanography* 19, 1–15. <http://dx.doi.org/10.1029/2004PA001003>.
- Mohtadi, M., Rossel, P., Lange, C., Pantoja, S., Boning, P., Repeta, D., Grunwald, M., Lamy, F., Hebbeln, D., Brumsack, H., 2008. Deglacial pattern of circulation and marine productivity in the upwelling region off central-south Chile. *Earth Planet. Sci. Lett.* 272, 221–230. <http://dx.doi.org/10.1016/j.epsl.2008.04.043>.
- Pelletier, J.D., Murray, A.B., Pierce, J.L., Bierman, P.R., Breshears, D.D., Crosby, B.T., Ellis, M., Foufoula-georgiou, E., Heimsath, A.M., Houser, C., Lancaster, N., Marani, M., Merritts, D.J., Moore, L.J., Pederson, J.L., Poulos, M.J., Rittenour, T.M., Rowland, J.C., Ruggiero, P., Ward, D.J., Wickert, A.D., Yager, E.M., 2015. Forecasting the response of Earth's surface to future climatic and land use changes: a review of methods and research needs. *Earth Futur.* 3, 220–251. <http://dx.doi.org/10.1002/2014EF000290>. Received.
- Piper, D.J.W., Normark, W.R., 2009. Processes that initiate turbidity currents and their influence on turbidites: a marine geology perspective. *J. Sediment. Res.* 79, 347–362. <http://dx.doi.org/10.2110/jsr.2009.046>.
- Pisias, N.G., Heusser, L., Heusser, C., Hostetler, S.W., Mix, A.C., Weber, M., 2006. Radiolaria and pollen records from 0 to 50 ka at ODP Site 1233: continental and marine climate records from the Southeast Pacific. *Quat. Sci. Rev.* 25, 455–473. <http://dx.doi.org/10.1016/j.quascirev.2005.06.009>.
- Rehak, K., Niedermann, S., Preusser, F., Strecker, M.R., Echter, H.P., 2010. Late Pleistocene landscape evolution in south-central Chile constrained by luminescence and stable cosmogenic nuclide dating. *Geol. Soc. Am. Bull.* 122, 1235–1247. <http://dx.doi.org/10.1130/B26545.1>.
- Reimer, P., Bard, E., Bayliss, A., 2013. IntCal13 and Marine13 radiocarbon age calibration curves 0–50,000 years cal BP. *Radiocarbon* 55, 1869–1887.
- Romans, B.W., Castellort, S., Covault, J.A., Fildani, A., Walsh, J.P., 2016. Environmental signal propagation in sedimentary systems across timescales. *Earth-Sci. Rev.* 153, 7–29. <http://dx.doi.org/10.1016/j.earscirev.2015.07.012>.
- Romans, B.W., Graham, S.A., 2013. A deep-time perspective of land–ocean linkages in the sedimentary record. *Annu. Rev. Mar. Sci.* 5, 69–94. <http://dx.doi.org/10.1146/annurev-marine-121211-172426>.
- Romans, B.W., Normark, W.R., McGann, M.M., Covault, J.A., Graham, S.A., 2009. Coarse-grained sediment delivery and distribution in the Holocene Santa Monica Basin, California: implications for evaluating source-to-sink flux at millennial time scales. *Geol. Soc. Am. Bull.* 121, 1394–1408. <http://dx.doi.org/10.1130/B26393.1>.
- Schumm, S.A., 1981. Evolution and response of the fluvial system. *SEPM Spec. Publ.* 19–29.
- Siani, G., Michel, E., De Pol-Holz, R., Devries, T., Lamy, F., Carel, M., Isguder, G., Dewilde, F., Lourantou, A., 2013. Carbon isotope records reveal precise timing of enhanced Southern Ocean upwelling during the last deglaciation. *Nat. Commun.* 4, 2758. <http://dx.doi.org/10.1038/ncomms3758>.
- Siddall, M., Rohling, E., Almogi-Labin, A., Hemleben, C., Meischner, D., Schmelzer, I., Smeed, D.A., 2003. Sea-level fluctuations during the last glacial cycle. *Nature* 423, 19–24. <http://dx.doi.org/10.1038/nature01687.1>.
- Simpson, G., Castellort, S., 2012. Model shows that rivers transmit high-frequency climate cycles to the sedimentary record. *Geology* 40, 1131–1134. <http://dx.doi.org/10.1130/G33451.1>.
- Sterken, M., Verleyen, E., Sabbe, K., Terryn, G., Charlet, F., Bertrand, S., Boës, X., Fagel, N., Batist, M., Vyverman, W., 2008. Late Quaternary climatic changes in southern Chile, as recorded in a diatom sequence of Lago Puyehue (40°40'S). *J. Paleolimnol.* 39, 219–235. <http://dx.doi.org/10.1007/s10933-007-9114-1>.
- Stuut, J.B.W., Lamy, F., 2004. Climate variability at the southern boundaries of the Namib (southwestern Africa) and Atacama (northern Chile) coastal deserts during the last 120,000 yr. *Quat. Res.* 62, 301–309. <http://dx.doi.org/10.1016/j.yqres.2004.08.001>.
- Suárez, M.D., Emparan, C., 1997. Hoja Curacautin – Regiones de la Araucanía y del Bio-Bío, Map 105, scale 1:250,000. Vergara, Santiago, Chile.
- Syvitski, J., Peckham, S.D., Hilberman, R., Mulder, T., 2003. Predicting the terrestrial flux of sediment to the global ocean: a planetary perspective. *Sediment. Geol.* 162, 5–24. [http://dx.doi.org/10.1016/S0037-0738\(03\)00232-X](http://dx.doi.org/10.1016/S0037-0738(03)00232-X).
- Talling, P.J., Amy, L.A., Wynn, R.B., 2007. New insight into the evolution of large-volume turbidity currents: comparison of turbidite shape and previous modelling results. *Sedimentology* 54, 737–769. <http://dx.doi.org/10.1111/j.1365-3091.2007.00858.x>.
- ten Brink, U.S., Andrews, B.D., Miller, N.C., 2016. Seismicity and sedimentation rate effects on submarine slope stability. *Geology* 44, 563–566. <http://dx.doi.org/10.1130/G37866.1>.
- Toucanne, S., Zaragosi, S., Bourillet, J.-F., Dennielou, B., Jorry, S.J., Jouet, G., Cremer, M., 2012. External controls on turbidite sedimentation on the glacially-influenced Armorican margin (Bay of Biscay, western European margin). *Mar. Geol.* 303–306, 137–153. <http://dx.doi.org/10.1016/j.margeo.2012.02.008>.
- Toucanne, S., Zaragosi, S., Bourillet, J.F., Gibbard, P.L., Eynaud, F., Giraudeau, J., Turon, J.L., Cremer, M., Cortijo, E., Martinez, P., Rössignol, L., 2009. A 1.2 Ma record of glaciation and fluvial discharge from the West European Atlantic margin. *Quat. Sci. Rev.* 28, 2974–2981. <http://dx.doi.org/10.1016/j.quascirev.2009.08.003>.
- Toucanne, S., Zaragosi, S., Bourillet, J.F., Naughton, F., Cremer, M., Eynaud, F., Dennielou, B., 2008. Activity of the turbidite levees of the Celtic–Armorican margin (Bay of Biscay) during the last 30,000 years: imprints of the last European deglaciation and Heinrich events. *Mar. Geol.* 247, 84–103. <http://dx.doi.org/10.1016/j.margeo.2007.08.006>.
- Valero-Garcés, B.L., Jenny, B., Rondanelli, M., Delgado-Huertas, A., Burns, S.J., Veit, H., Moreno, A., 2005. Palaeohydrology of Laguna de Tagua Tagua (34°30'S) and moisture fluctuations in Central Chile for the last 46 000 yr. *J. Quat. Sci.* 20, 625–641. <http://dx.doi.org/10.1002/jqs.988>.
- Veit, H., 1996. Southern Westerlies during the Holocene deduced from geomorphological and pedological studies in the Norte Chico, Northern Chile (27°–33°S). *Palaeogeogr. Palaeoclimatol. Palaeoecol.* 123, 107–119. [http://dx.doi.org/10.1016/0031-0182\(95\)00118-2](http://dx.doi.org/10.1016/0031-0182(95)00118-2).
- Völker, D., Geersen, J., Contreras-Reyes, E., Reichert, C., 2013. Sedimentary fill of the Chile Trench (32°–46°S): volumetric distribution and causal factors. *J. Geol. Soc. Lond.* 170, 723–736. <http://dx.doi.org/10.1144/jgs2012-119>.
- Völker, D., Geersen, J., Contreras-Reyes, E., Sellanes, J., Pantoja, S., Rabbal, W., Thorwart, M., Reichert, C., Block, M., Weinrebe, W.R., 2014. Morphology and geology of the continental shelf and upper slope of southern Central Chile (33°S–43°S). *Int. J. Earth Sci.* 103, 1765–1787. <http://dx.doi.org/10.1007/s00531-012-0795-y>.
- Völker, D., Reichel, T., Wiedicke, M., Heubeck, C., 2008. Turbidites deposited on Southern Central Chilean seamounts: evidence for energetic turbidity currents. *Mar. Geol.* 251, 15–31. <http://dx.doi.org/10.1016/j.margeo.2008.01.008>.
- Wang, Y., Straub, K.M., Hajek, A.E., 2011. Scale-dependent compensational stacking: an estimate of autogenic time scales in channelized sedimentary deposits. *Geology* 39, 811–814. <http://dx.doi.org/10.1130/G32068.1>.
- Weltje, G.J., 1997. End-member modeling of compositional data: numerical-statistical algorithms for solving the explicit mixing problem. *Math. Geol.* 29, 503–549. <http://dx.doi.org/10.1007/BF02775085>.
- Zech, R., Kull, C., Kubik, P.W., Veit, H., 2006. Exposure dating of Late Glacial and pre-LGM moraines in the Cordón de Doña Rosa, Northern/Central Chile (~31°S). *Clim. Past* 2, 847–878. <http://dx.doi.org/10.5194/cpd-2-847-2006>.